



# Evaluating the radiative fidelity of PALM (v25.04) in high-resolution: impact of diverse urban morphology and vegetation on short-wave radiation

Jelena Radović<sup>1</sup>, Michal Belda<sup>1</sup>, Martin Bureš<sup>2</sup>, Kryštof Eben<sup>2</sup>, Jan Geletič<sup>1,2</sup>, Jakub Jura<sup>3</sup>, Pavel Krč<sup>2</sup>, Hynek Řezníček<sup>2</sup>, and Jaroslav Resler<sup>2</sup>

<sup>1</sup>Department of Atmospheric Physics, Faculty of Mathematics and Physics, Charles University Prague, V Holešovičkách 2, 180 00 Prague 8, Czech Republic

<sup>2</sup>Department of Complex Systems, Institute of Computer Science of the Czech Academy of Sciences, Pod Vodárenskou věží 271/2, 182 00 Prague, Czech Republic

<sup>3</sup>Department of Instrumentation and Control Engineering, Faculty of Mechanical Engineering, Czech Technical University in Prague, Technická 4, 166 07 Praha 6, Czech Republic

**Correspondence:** Jelena Radović (jelena.radovic@matfyz.cuni.cz)

**Abstract.** Validating short-wave radiation in numerical models is non-trivial, as city measurements are heavily influenced by multiple reflections, absorption, and shading processes driven by the three-dimensional urban morphology and vegetation. At the same time, urban micro-scale models are typically forced by only two types of solar radiation inputs: i) field measurements, often represented by the global radiation, rarely by the combination of short-wave and long-wave radiation; and ii) data given from coarser-resolution models. We conduct a novel high-resolution evaluation study of the PALM model (v25.04), driven by the regional WRF model configured in two distinct parameterisation setups, across a multi-episode ensemble spanning from clear-sky to overcast conditions. We validate and quantify PALM's ability to explicitly resolve the spatiotemporal propagation of short-wave radiation and its interaction with heterogeneous urban landscapes against measurements collected from the stations located in morphologically variant urban settings with different solar access. Results demonstrate that PALM resolves urban- and vegetation-induced short-wave radiative exchange (i.e., canyon trapping, vegetation shading, building reflections, interaction with urban surfaces and dynamic timing) with high fidelity regardless of the urban setting, a capability that meso-scale models cannot match. The study reveals the dominant role of biases: despite PALM's superiority, the errors embedded in meso-scale cloud fields and radiation inputs cannot be fully compensated for by the micro-scale model. This work is a benchmark for the validation of high-resolution urban radiative transfer exchanges and shows that future progress in street-scale micrometeorological simulations hinges on rigorous verification of cloud representation and radiative fields in the meso-scale driving data.

## 1 Introduction

Proper assessment of urban environments using high-resolution environmental prediction models is a prerequisite for improving the well-being of urban dwellers in densely populated built-up areas (Baklanov et al., 2018). The ever-increasing



20 urbanisation (United Nations, 2024), combined with climate change and continuous urban development, is exacerbating exist-  
ing environmental hazards, such as increased heat stress, disrupted thermal comfort, air pollution, and water scarcity (Lehnert  
et al., 2023; Vieira Zezzo et al., 2023). Cities comprise complex urban structures with numerous land-cover components (e.g.,  
urban fabric, transit roads, green spaces, water bodies, sports and leisure facilities). Such a configuration of cities alters and  
unevenly distributes incoming short-wave radiation from the Sun, thereby affecting radiative exchange processes within the  
25 urban boundary layer (Freitas et al., 2015; Oke et al., 2017; Liu et al., 2020; Krč et al., 2021; Geletič et al., 2023; Schoetter  
et al., 2023). The specific set of interactions with incident solar radiation associated with urban trees primarily involves shad-  
ing, transpiration, and effects on air temperature, among other factors (Wang and Akbari, 2016; Chen et al., 2021; Geletič et al.,  
2022; Grylls and van Reeuwijk, 2022).

The aforementioned properties of cities exacerbate an already complex process of modelling urban areas and climate, particu-  
30 larly with respect to radiative processes. As spatial resolution increases, the complexity of radiative processes increases.  
The necessity of a proper understanding of radiation exchange processes in urban environments has been recognised by World  
Meteorological Organization (2024), and the need for their accurate representation in numerical models designed for the ur-  
ban boundary layer has been highlighted by Krč et al. (2021). Given the complexity of a micro-scale urban environment, it is  
necessary to consider the interactions of buildings and vegetation with short- and long-wave radiation, as well as reflection,  
35 scattering, and thermal emission (Salim et al., 2022). The accurate evaluation of the sky view factor (SVF; Krč et al., 2021) is  
another important aspect of the radiative transfer model (RTM) since it strongly influences the amount of incoming radiation  
(Gál and Kántor, 2020). Thus, the SVF influences the surface radiation balance and is a key component in describing urban  
climatology at scales below 100 m (Dirksen et al., 2019). Since the SVF affects the interaction of short-wave and long-wave  
radiation from the sky and the surface, its proper estimation by numerical models is necessary (Salim et al., 2022).

40 Recently, in the practical application of high-fidelity modelling results, there has been increasing demand from urban plan-  
ners, architects, and municipalities for the estimation of biometeorological indices (Matzarakis et al., 2010; Jänicke et al.,  
2015; Geletič et al., 2021). However, most of these indices are strongly dependent on radiation, typically expressed as mean  
radiant temperature (MRT; Krč et al., 2021). According to Wallenberg et al. (2020), MRT is the most significant meteorological  
variable affecting human energy balance and thermal comfort on clear, sunny days. Outdoor MRT combines the impacts of  
45 short-wave and long-wave radiation in outdoor environments. While long-wave dominates indoor environments, short-wave ra-  
diation is often the primary driver of high MRT values outdoors, especially at high solar altitudes. MRT is directly derived from  
the short-wave radiation flux density and is governed by the short-wave radiation flux (Lee et al., 2014). Short-wave outdoor  
MRT includes all components of solar radiation: direct, reflected (from surfaces), and sky-diffused radiation. MRT is further  
used for the calculation of other biometeorological indices, such as predicted mean vote (PMV; Fanger, 1967), physiologically  
50 equivalent temperature (PET; Höppe, 1999), or universal thermal climate index (UTCI; Jendritzky et al., 2012). Given these  
facts, it is essential to accurately simulate short-wave radiation in the numerical model (Matzarakis et al., 2010).

The theoretical basis and the level of sophistication achieved in the modelling approaches vary across models. For example, a  
relatively simple one-dimensional diagnostic micro-scale model named RayMan, developed by Matzarakis et al. (2007, 2010),  
can calculate radiation fluxes in urban environments with resolved buildings and trees. The model computes the SVF and MRT



55 required for thermal index calculation (e.g., Middel et al., 2017; Fröhlich et al., 2019). RayMan's further development is the steady-state SkyHelios model, which incorporates spatial dimensions and indirect effects of wind velocity on long-wave radiation within the computational domain (e.g., Matuschek and Matzarakis, 2011; Fröhlich and Matzarakis, 2018; Fröhlich et al., 2019). The Solar and long-wave Environmental Irradiance Geometry (SOLWEIG) is another widely used microclimate model for assessing urban radiative processes (Lindberg et al., 2008), which, unlike the models above, simulates the spatiotemporal  
60 distribution of radiation fluxes. The SOLWEIG model has been the subject of numerous studies evaluating its performance in simulating radiation fluxes and MRT (Chen et al., 2016; Kántor et al., 2018; Aminipouri et al., 2019; Gál and Kántor, 2020). A more advanced method for assessing urban environments and microclimates is the use of Computational Fluid Dynamics (CFD) models, which, according to Yang et al. (2023), are widely employed for this purpose. CFD models can simulate a variety of spatial and temporal scales, resolving physical processes and the city's topography (e.g., buildings, trees) in great  
65 detail (Blocken, 2015, 2018; Toparlak et al., 2017; Kubilay et al., 2020). In the CFD space, several models with strong competence and different approaches to assessing radiation transfer processes have emerged: ENVI-met (Bruse et al., 2023a, b), City-LES (Kusaka et al., 2024), the Parallelized Large-Eddy Simulation Model (PALM) (Maronga et al., 2020), or uDALES (Suter et al., 2022). Validation of the ENVI-met's short-wave radiation fluxes has been performed by Jänicke et al. (2015) and of the global radiation by Liu et al. (2018) and Piselli et al. (2018). Gál and Kántor (2020) and Liu et al. (2020) compared  
70 RayMan, SOLWEIG, and ENVI-met micro-scale models; both studies show that the SOLWEIG model is the most accurate and RayMan the least accurate among the three models. Moreover, the study by Liu et al. (2020) highlights the strengths and shortcomings of the models and their capabilities for assessing urban radiation fields.

The meteorological model City-LES can simulate radiative transfer processes in urban environments at high spatial resolution. The latest improvements in the City-LES model are described in Watanabe et al. (2022) and Kusaka et al. (2024).  
75 This model can resolve shadows from buildings and trees, incorporate cloud physics and atmospheric radiation models such as RRTM, and, using the radiosity method (Aoyagi and Takahashi, 2012), account for multiple reflections of short-wave and long-wave radiation between buildings or trees. The numerical schemes representing radiation processes available in the City-LES model are as follows: i) short-wave radiation can be modelled by the Kondo (1994) scheme or the Dudhia simple scheme (Dudhia, 1989); ii) long-wave radiation is modelled either by Kondo (1994) scheme or the RRTM scheme (Mlawer et al.,  
80 1997); iii) radiation within the urban canopy layer is modelled by the radiosity method (Aoyagi and Takahashi, 2012). The uDALES model, recently developed by Suter et al. (2022), also accounts for all governing processes in the urban environment (e.g., vegetation effects, energy and momentum fluxes from urban surfaces, radiation, etc.). For radiation processes, it applies the method of Rao and Sastri (1996) to calculate view factors between planar surfaces and utilises these view factors for both short-wave and long-wave radiation calculations. Similar to City-LES and the first version of RTM (Resler et al., 2017) in  
85 PALM, uDALES employs the radiosity method (Aoyagi and Takahashi, 2012) to model short-wave and long-wave radiative fluxes within the urban canopy layer. We refer to Suter et al. (2022) for further details on uDALES radiative transfer modelling.

The PALM model system offers a variety of techniques for radiation process modelling. The radiation can be prescribed as constant in the configuration, or a realistic diurnal cycle can be modelled by the internal clear-sky model or by the coupled rapid radiative transfer model (RRTM; Hogan and Bozzo, 2018). It is also possible to use values from an external model or



90 measurements supplied in the dynamic driver (initial and boundary condition provider). Interactions of the radiation with the  
surface (ground, buildings) and plant canopy are modelled by the integrated RTM (Krč et al., 2021). Alternatively, the ex-  
ternally coupled TenStream model (Jakub and Mayer, 2016) can be used. Starting with the simple one-dimensional radiation  
model, which takes into account only vertical radiation exchange (Maronga et al., 2015), then moving to more complicated op-  
tions such as the clear-sky model (Maronga et al., 2020), RRTM for general circulation models (RRTMG; Clough et al., 2005)  
95 and RTM (Resler et al., 2017; Krč et al., 2021). The last published version of RTM (3.0) (Krč et al., 2021), based on RTM  
version 1.0 (Resler et al., 2017), explicitly resolves radiative processes in three-dimensional, complex urban environments  
at street-scale resolutions of meters. Beyond RTM's capability for high-fidelity, what distinguishes PALM from other estab-  
lished microscale models is the methodological coherence it maintains between radiation physics and the initial and boundary  
conditions governing boundary-layer dynamics. Namely, reproducing the spatio-temporal variability of urban boundary-layer  
100 conditions -particularly radiative conditions and associated quantities- with microscale models like City-LES and uDALES, is  
limited by their atmospheric dynamics initialisation procedures. These modelling frameworks are not designed to work with  
arbitrarily chosen, temporally evolving, three-dimensional meteorological fields downscaled from meso-scale models; instead,  
they rely on observational forcing, commonly supplied through measured vertical profiles. On the other hand, this imperative of  
achieving physical consistency and bridging the atmospheric meso-micro scale-gap is satisfied by PALM's meso-scale nesting  
105 (MESO; Kadasch et al., 2021) model,

Previous studies, such as (Resler et al., 2017, 2021; Krč et al., 2021), validated the RTM against observations, while Salim  
et al. (2022) explored the significance of radiative transfer processes by systematically isolating them in the PALM model. It is  
worth noting that the direct evaluation of the radiation model using field measurements has not yet been conducted. The studies  
mentioned above indirectly assess radiation processes by examining surface temperatures, which strongly depend on accurate  
110 radiation. Hence, the primary objective of this study is the validation of PALM's ability to simulate short-wave radiation and  
the investigation of how it modifies both direct and reflected short-wave radiation by comparing four different locations within  
the simulation domain. Following the validation, the micro-scale effects of vegetation and buildings on short-wave radiation in  
a realistic urban environment are examined. Lastly, uncertainties related to the urban environment or input data are addressed.

This paper is structured as follows. The PALM model configuration and the radiative transfer model are explained in Section.  
115 2.1 and Sect. 2.1.1, respectively. Initial and boundary conditions used for simulations are described in Section 2.2, followed  
by the domain description (Sect. 2.3), measurement description (Sect. 2.4), simulated episodes (Sect. 2.5), and experiment  
workflow in Section 2.7. In section 3, we present the results. Lastly, Sections 4 and 5 present the discussion and conclusion,  
respectively.

## 2 Methodology

### 120 2.1 PALM model configuration

The micro-scale simulations were performed using the PALM model system (Maronga et al., 2020) in version 25.04 (see Data  
availability section). The aforementioned model is a turbulence-resolving LES micro-scale meteorological model developed to



support urban boundary-layer and climate research (Maronga et al., 2015, 2020). By employing the non-hydrostatic, filtered, Boussinesq-approximated incompressible Navier–Stokes equations together with a suite of specially developed components (see e.g., Maronga et al. (2020)), this numerical framework serves as a robust tool for theoretical and practical evaluation of the urban atmosphere at the street scale. Due to its extensible architecture, PALM can be configured for specific applications; for example, when wind dynamics are not required, as in simulations focused solely on short-wave solar radiation, the model can be run in spin-up mode. This arrangement greatly lowers computational requirements while still allowing for the evaluation and running of a larger number of configurations and parameterisations. Rather than relying on accumulated resolved heat inputs, the spin-up phase is predominantly driven by the prescribed diurnal temperature cycle, which affects the surface energy balance and effectively enables the surface heat transfer and storage model to approach real conditions. Spin-up has a strong impact on long-wave radiation but no effect on short-wave radiation. Radiation and geometric effects-such as shadings from buildings or trees, multiple reflections, and view factors-are still included in the simulation. Depending on the configuration, the primary radiative forcing is provided either by a model integrated in PALM (such as RRTMG) or, as in this study, by external forcing from the dynamic driver file. The dynamic driver values are usually obtained either from a meso-scale model, such as WRF, or from measured values. The surface energy balance is solved using Land Surface Model (LSM; Gehrke et al., 2021), Building Surface Model (BSM; Resler et al., 2017; Maronga et al., 2020), and radiative Transfer Model and Plant Canopy Model (RTM and PCM; Krč et al., 2021) with the static driver, without the need for LES. As a result, any biases in the simulated short-wave radiation will be caused by driver errors, geometry effects (sky view factor), or incorrect input parameters. The present experimental setup utilises a pre-validated urban simulation domain of Dejvice, Prague (Resler et al., 2021). Micro-scale simulations were executed in the spin-up methodology described above, while the modules employed in this study are the LSM, BSM, RTM and MESO.

### 2.1.1 RTM configuration

The RTM version used in this study is 4.1, which utilises a ray-tracing algorithm for handling fully 3D structures, including downward-facing faces, which differs from RTM 3.0, which operates by default on 2.5D geometry. The new localised ray-tracing parallelisation algorithm for calculating sky view factors, introduced in version 4.0, was employed. To identify all the rays affecting each grid cell, the angular discretisation algorithm (Krč et al., 2021, section 2.2) is used. The default settings are 4.5 degrees in zenith and azimuthal direction (40 zenith angles and 80 azimuth angles, resulting in a total of 3,200 possible directions). For experimental purposes, the RTM's external radiation scheme option was utilised, which uses the meso-scale model WRF's 10-minute outputs for external radiative input data (i.e., short- and long-wave downwelling radiation).

### 2.2 Initial and boundary conditions

For the radiation initial and boundary conditions, the Weather Research and Forecasting (WRF) model (Skamarock et al., 2019) in versions 4.4 (WRF-CNU setup; denoted interchangeably as CNU) and 4.6.1 (WRF-FU setup, denoted interchangeably as FU) was employed. WRF is a widely used, state-of-the-art meso-scale numerical weather prediction system designed for both atmospheric research and operational forecasting. It comprises two dynamical cores, a data assimilation system, and a software



architecture that supports parallel computation and system extensibility. The model serves a wide range of meteorological applications across scales, from tens of meters to thousands of kilometres, and, together with field measurements, can serve as input forcing for micro-scale simulations.

The dynamic meteorological forcing in this study is derived from two different WRF model setups: a coarse-resolution non-urban setup (WRF-CNU; 3 km horizontal resolution), and a fine-resolution urban setup (WRF-FU; 1 km horizontal resolution). A comparative overview of the physics schemes for both WRF configurations is summarised in Table 1. Typically, the main WRF output files contain data at 1-hour intervals. However, when addressing radiation modelling in the context of changes in solar irradiance and the likelihood of cloud development and movement, it is preferable to configure WRF to generate auxiliary output files containing only radiation-related variables at a finer temporal resolution (e.g., 10 minutes). Furthermore, the WRF files for the PALM-meteo (the preprocessor of meso-scale meteorology which generates the PALM dynamic driver; see Krč et al., 2025) need to contain short-wave and long-wave horizontal irradiance (marked in WRF as downward radiation); the diffuse component of the short-wave horizontal irradiance is optional. If this component is absent, it is skipped during dynamic driver preprocessing, and the PALM radiation module uses its internal estimate of the direct-to-diffuse ratio. When utilising a high-resolution model such as PALM, it is preferable to introduce the input data in high quality (Radović et al., 2024). Hence, for radiation, this study uses 10-minute WRF radiation data to drive the PALM model.

**Table 1.** WRF parametrisation schemes utilized in the experiment.

Physics Scheme	WRF-CNU <sup>1</sup>	WRF-FU <sup>2</sup>
Planetary Boundary Layer	MYNN Level 2.5 (Nakanishi and Niino, 2009)	Bougeault–Lacarrere Scheme (BouLac; Bougeault and Lacarrere, 1989)
Urban Physics	0 (disabled)	Building Energy Model (BEM; Salamanca and Martilli, 2009)
Long-wave radiation	RRTMG (Iacono et al., 2008)	RRTMG (Iacono et al., 2008)
Short-wave radiation	RRTMG (Iacono et al., 2008)	RRTMG (Iacono et al., 2008)
Surface layer	Revised MM5 Scheme (Jimenez et al., 2012)	Revised MM5 Scheme (Jimenez et al., 2012)
Land Surface	Unified Noah Land Surface Model (Tewari et al., 2004)	Unified Noah Land Surface Model (Tewari et al., 2004)
Microphysics	Thompson (Thompson et al., 2008)	Thompson (Thompson et al., 2008)

<sup>1</sup> Coarse-resolution non-urban setup–WRF-CNU (3 km horizontal resolution)

<sup>2</sup> Fine-resolution urban setup–WRF-FU (1 km horizontal resolution)

### 2.3 Study area description

The study area is located in Dejvice, a district of Prague, the capital of the Czech Republic. As presented in Holtanová et al. (2025), Prague is in a temperate continental climate zone.



The average annual air temperature recorded at the meteorological station Praha-Klementinum (WMO ID 11515, located  
175 in the city centre) was 11.5 °C, according to the WMO’s Climatological Standard Normal for 1991–2020. The mean air  
temperature in July, typically the warmest month, was 21.6 °C. The coldest month, with a temperature of 1.8 °C, is typically  
January. Average annual precipitation is 453.9 mm, and mean monthly sunshine hours range from 46.2 (December) to 229.1  
(July).

There are four major types of built-up areas in Dejvice (Fig. 1) with the following Local Climate Zone (LCZ; Stewart and  
180 Oke, 2012) classification: 1) historical residential areas in south-east, classified as LCZ 2 Compact midrise, 2) a combination  
of old and new buildings with a variety of other urban components (west and north-west), predominantly classified as LCZ 5  
Open midrise, 3) a residential area with green gardens (north-east) that corresponds to LCZ 6 Open lowrise, and 4) lightly  
wooded landscape of deciduous trees, with a grass sublayer (LCZ B Scattered trees; more precisely in the case of Hanspaulka  
(HAN) observational station (see Fig. 1), the transitional class LCZ B<sub>D</sub>).

## 185 2.4 Measurement campaign and observational dataset

Measurement locations (see Fig. 1) were situated in the north-west of Dejvice, mainly in the Czech Technical University  
campus. There were two calibrated stations, each producing 10-minute averages for two years (2017–2018). At the end of  
the year 2017, both stations were moved to a new position (four locations in total; see Table 2) (Jura et al., 2018). The first  
location, opened in 2017, was situated on the asphalt surface (FSV) and was primarily influenced by the surrounding buildings.  
190 The effect of the plant canopy, distanced  $\approx 20$  m with an approximate crown perimeter of 2 m, was negligible in most cases.  
The second position in 2017 was in a public orchard with fruit trees (HAN). The station surroundings were affected during the  
vegetation season by various grass heights (0.2–1.0 m) and available soil moisture. The majority of fruit trees were lower than  
4 m and were distanced more than 5 m from the measurement location. The third location, first in 2018, was in a small park  
known as Fleming Square (FLE). The station was situated on a homogeneous grass surface and was significantly impacted  
195 by neighbouring trees. The last location (NTK), second in 2018, was situated on light grey coloured concrete, between the  
National Technical Library building and a tree alley (height 8–10 m) on the south-west. An additional note pertains to the  
curved glassy walls of the neighbouring library, which, under specific conditions, can reflect incoming short-wave radiation.

**Table 2.** Measurement locations in Prague-Dejvice

Name	Coordinates (latitude, longitude)	Year	Surface albedo
FLE	50.1049783 N, 14.3917394 E	2017	0.173
NTK	50.1034739 N, 14.3905364 E	2017	0.247
FSV	50.1039264 N, 14.3892972 E	2018	0.120
HAN	50.1052408 N, 14.3825917 E	2018	0.170

Each measurement station was equipped with several sensors: two RVT 11 for air temperature and relative humidity (at  
heights of 0.3 and 2.0 m), three Pt<sub>100</sub> for soil temperature (at various depths), a “Tlust’ák W2” anemometer for wind speed and

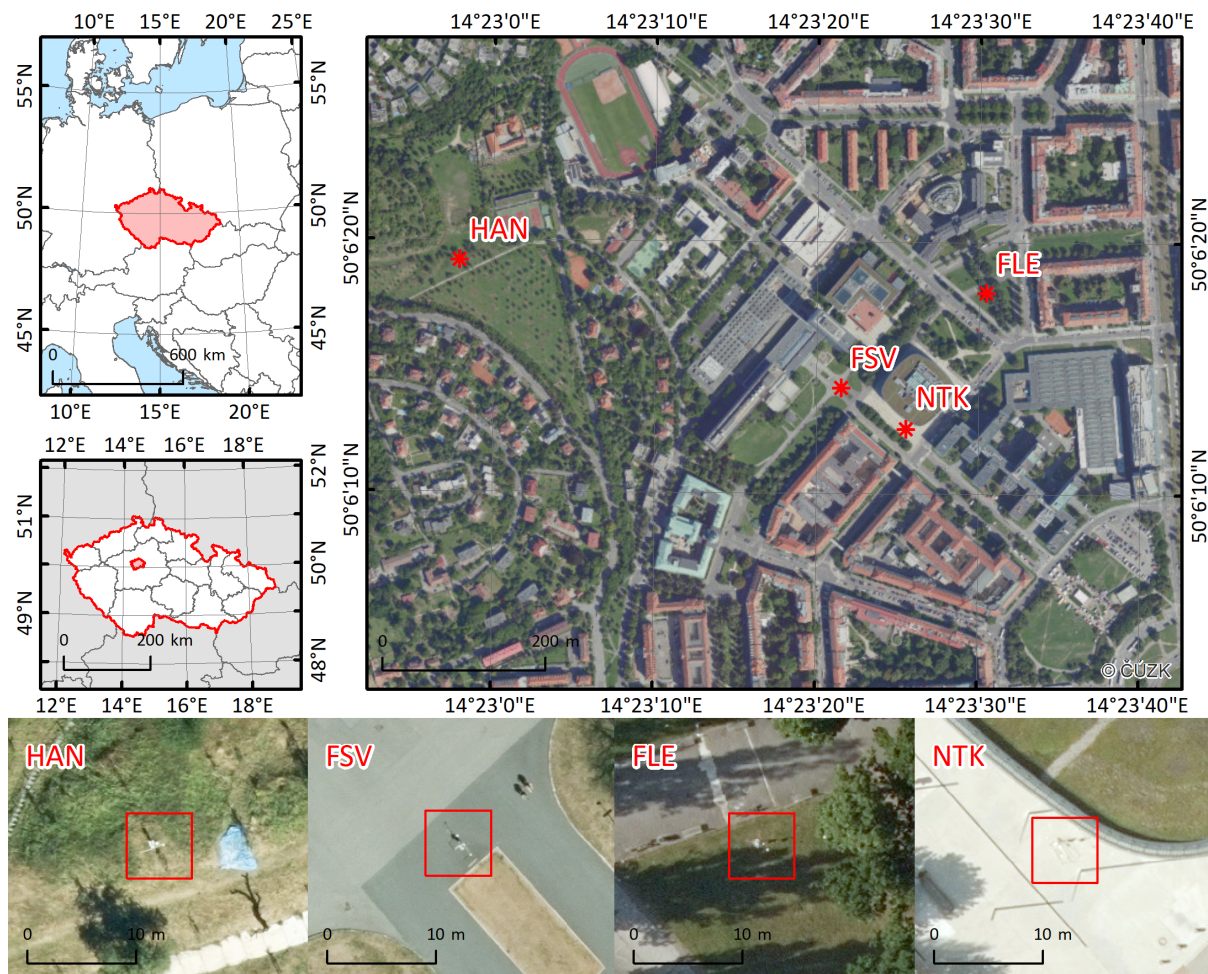


**Figure 1.** The position of the domain in Central Europe (top left) and the Czech Republic (middle left). Red stars indicate measurement location. The orthophotography on the top right map was provided by the Czech Cadastral Office © via the web map service. The bottom figures represent the individual station locations (red squares) in 2017 and 2018. The orthophotographs for year-specific locations were provided by the Prague Institute of Planning and Development (IPR) ©. Note that IPR orthophotographs are from a perspective view.

200 direction, and two Kipp&Zonen CMP3 pyranometers with the spectral range from 300 to 2,800 nm for incoming and reflected solar radiation. The pyranometer's interval covers most of the short-wave radiation spectrum, although not the entire spectrum; in the following text, its results as a short-wave radiation measurement will be considered. Details about sensors are available in Table 3 or Jura et al. (2018).



**Table 3.** Sensors on the measuring stations and their technical parameters. Surface albedo values were calculated using measurements in Jura et al. (2018).

Sensor	Variables	Range	Typical accuracy	Resolution
Kipp&Zonen CMP3	global radiation (income)	0–1,500 Wm <sup>-2</sup>	0.006 Wm <sup>-2</sup>	16.30 Wm <sup>-2</sup>
	global radiation (reflected)	0–1,500 Wm <sup>-2</sup>	1.040 Wm <sup>-2</sup>	0.65 Wm <sup>-2</sup>
RVT 11	air temperature	–40 to 60 °C	±0.33 °C	0.03 °C
	relative humidity	0–100 %	±1.85 %	0.47 %
Tlust’ák W2	wind direction	0–360 °	10 °	1 °
	wind speed	0–30 ms <sup>-1</sup>	0.5 ms <sup>-1</sup>	0.1 ms <sup>-1</sup>
Pt <sub>100</sub>	soil temperature	–40 to 60 °C	±0.33 °C	0.03 °C

## 2.5 Simulation episodes and meteorological conditions

205 Atmospheric conditions with no cloud cover, or the so-called “clear-sky” days, characterised by a smooth, parabolic-shaped  
 curve, are an ideal testbed for evaluating radiation physics in micro-scale models like PALM thanks to a high confidence  
 in the incoming solar radiation. Nevertheless, high-solar-irradiance weather conditions with a completely cloud-free sky are  
 relatively rare; more realistic conditions involve heterogeneous variations of thin cirrus, scattered cumulus, or cloud fragments.  
 To cover a series of typical summer heat wave periods and the corresponding atmospheric radiation regimes, a total of 16  
 210 episodes with various types of synoptic and cloud cover conditions during the summers of 2017 and 2018 were selected  
 for model evaluation. Since the chosen episodes differ in cloud cover, they are categorised into two groups: predominantly  
 cloud-free episodes, referred to as “clear-sky” (i.e., clear-sky proxies), and episodes with pronounced cloudiness, referred to  
 as “non-clear-sky” episodes. Simulation episodes cover a range of large-scale weather systems and fronts crossing Prague  
 (e.g., cyclonic and anticyclonic), providing a realistic set of meteorological conditions (see Table S1). Six of the 16 episodes  
 215 (e1–e6) serve as a sample for the direct WRF setup-to-setup intercomparison (i.e., CNU vs. FU). To further validate the WRF-  
 FU’s setup generalisability and transferability and to deliver a more robust statistical evaluation, the analysis was extended to  
 10 additional episodes (e7–e16) simulated using the WRF-FU setup only. Comprehensive details on the simulation episodes,  
 cloud conditions, and associated WRF driving configurations are provided in Table 4.



**Table 4.** Overview of simulation episodes, cloud conditions, and WRF configurations used in the study. The six common episodes (e1–e6) used for direct comparison were simulated with both the Coarse No Urban (WRF-CNU) and Fine Urban (WRF-FU) configurations, while the additional episodes (e7–e16) were simulated only with the FU configuration.

Episode	Date	Cloud conditions	Category	CNU	FU
<b>Common episodes</b>					
e1	19–20/06/2017	clear-sky	Common	✓	✓
e2	19/07/2017	clear-sky	Common	✓	✓
e3	07/08/2017	clear-sky	Common	✓	✓
e4	30/06/2018	clear-sky	Common	✓	✓
e5	02–03/07/2018	clear-sky	Common	✓	✓
e6	11–12/09/2018	clear-sky	Common	✓	✓
<b>Additional episodes</b>					
e7	09/06/2017	clear-sky	FU-only	–	✓
e8	11/06/2017	clear-sky	FU-only	–	✓
e9	07/07/2017	non-clear-sky	FU-only	–	✓
e10	16/06/2018	non-clear-sky	FU-only	–	✓
e11	07/07/2018	clear-sky	FU-only	–	✓
e12	21/07/2018	non-clear-sky	FU-only	–	✓
e13	24/07/2018	clear-sky	FU-only	–	✓
e14	01/08/2018	clear-sky	FU-only	–	✓
e15	17/08/2018	clear-sky	FU-only	–	✓
e16	20/08/2018	clear-sky	FU-only	–	✓

## 2.6 PALM output and observation data processing

220 PALM output data are produced every 60 s relative to the simulation start. For each simulation episode, incoming and outgoing  
short-wave radiation fluxes (SWin and SWout) are extracted at the locations of the observation stations and averaged into hourly  
mean values. Similarly, measurements (recorded at 10 min intervals) were aggregated into hourly means. The obtained datasets  
for both variables are further distinguished by WRF driver (CNU and FU) and station. All subsequent analyses (statistical  
metrics, summary mean bias and root mean square error heatmaps, and scatter plots) are derived from these model/observation  
225 hourly data. To produce the overall Mean Bias Error (MBE) and Root Mean Square Error (RMSE) heatmaps, twofold averaging  
was performed: first, per episode (single episode-station-variable-WRF driver value), and then across all episodes (Fig. 2). In  
the scatter plots (Fig. 3 and Fig. 4), each point represents an hourly value of a variable at a specific observation station and  
WRF driver.



### 3 Results

230 The outcome of our simulations emphasises the link between meso-scale driving data and PALM micro-scale radiation process  
modelling. As shown in Radović et al. (2024), PALM performance largely depends on the quality of the forcing fields, whose  
features (e.g., general structure and biases) propagate into the micro-scale simulation, further affecting modelled variables.  
In order to describe the particular impact of forcing fields on short-wave radiative fluxes, PALM's response to the two dis-  
235 tinct WRF model setups is quantified. The general pattern between PALM and the corresponding observed radiation-related  
variables is identified (Fig. 3 and Fig. 4). To target differences and patterns between modelled and observed values, the data  
are clustered by WRF driver, cloud conditions, variables, and stations. The data are further processed, and the direction and  
magnitude of errors are quantified (Fig. 2).

#### 3.1 An overall view of the simulations

The influence of sky conditions and the configuration of driving data on PALM simulations is reflected in both absolute  
240 and relative metrics defined in Supplement Section 1 (see the differences in Tab. 5). Under non-clear-sky episodes (see, e.g.,  
column Non-clear (FU) in Tab. 5), and for all stations considered, SWin exhibits consistently large errors, with average absolute  
differences above  $80 \text{ Wm}^{-2}$  and average relative differences exceeding 100 %. The strongest degradation occurs at the NTK  
station, with a relative difference of 276.6 %, and at the FLE station, with an increase of over 100 %. These are station-specific  
anomalies that are not observed at the other two locations. The modelling of SWout is only slightly affected, as the increase  
245 in discrepancies is not substantial, except at the NTK station. On the other hand, PALM's fidelity improves for the clear-sky  
scenario simulated with the FU configuration, with both examined variables exhibiting comparatively small biases. However,  
the HAN station exhibits large relative and absolute differences, a pattern that holds across all sky conditions and driving data  
configurations. A more detailed analysis of the HAN station is presented in Section 3.2.2. The metrics quantifying the impact  
of the WRF configurations on SWin indicate that the FU outperforms the CNU, as the overall absolute difference decreases  
250 from  $67.9 \text{ Wm}^{-2}$  (CNU) to  $39.8 \text{ Wm}^{-2}$  (FU; corresponding to a reduction of roughly 40 %). Compared with SWin, WRF-FU  
improves SWout only at urban stations (FSV and NTK), whereas biases persist at vegetated sites (HAN and FLE), resulting in  
similar overall relative and absolute differences.

Given the performance metrics indicated by the Person's correlation coefficient  $r$ , Spearman's  $\rho$ , and Willmott's index of  
agreement  $d$ , the timing and magnitude of the modelled and observed values for SWin show a satisfactory agreement for both  
255 of the driving data configurations considered ( $r \approx 0.985$ ,  $\rho \approx 0.984$ ,  $d \geq 0.980$ ; see Tab. 6; metrics are defined in Supplement  
Section 1). An evaluation of all indicators, however, suggests that the FU configuration performs somewhat better than the  
CNU setup, particularly at urban stations (i.e., FSV and NTK). Outgoing short-wave radiation (SWout) shows a greater spread  
in performance metrics than SWin. There is a pronounced systematic bias in SWout at the HAN site, as indicated by low  
correlation and agreement metrics, and the strongly negative coefficient of determination ( $R^2 \approx -1.4$ ). This bias is consistent  
260 across the full analysis and in every tested configuration, indicating that the dominant source of error lies in the surface  
representation at HAN rather than in the driving data forcings alone. When examining PALM's performance under different



**Table 5.** Absolute and relative differences (%) for PALM-simulated incoming (SWin) and outgoing (SWout) short-wave radiation, evaluated across four measurement stations (FSV, NTK, HAN, and FLE). The results are categorised by sky conditions (Clear vs. Non-clear) and by WRF driving configurations (FU and CNU; see Table 4).

Station	Variable	Non-clear (FU)	Clear (FU)	Common (CNU)	Common (FU)
FSV	SWin	74.0 (19.3 %)	37.8 (−2.5 %)	78.2 (1.6 %)	43.4 (1.3 %)
	SWout	10.7 (4.3 %)	10.6 (−10.4 %)	15.6 (−16.8 %)	11.6 (−11.7 %)
NTK	SWin	163.8 (276.6 %)	38.0 (17.0 %)	81.2 (1.2 %)	33.5 (10.2 %)
	SWout	37.7 (163.3 %)	14.3 (−2.1 %)	28.2 (−15.7 %)	16.2 (−7.6 %)
HAN	SWin	59.2 (24.0 %)	31.5 (9.0 %)	53.2 (−4.7 %)	31.9 (5.1 %)
	SWout	53.6 (−38.6 %)	56.8 (−52.9 %)	56.8 (−52.6 %)	56.5 (−52.9 %)
FLE	SWin	96.0 (110.6 %)	56.7 (−1.3 %)	58.9 (9.7 %)	50.3 (−2.2 %)
	SWout	15.0 (1.9 %)	12.2 (−3.6 %)	11.7 (−3.1 %)	11.6 (−4.1 %)
Overall	SWin	87.7 (107.6 %)	39.5 (5.0 %)	67.9 (2.0 %)	39.8 (3.6 %)
	SWout	30.2 (32.7 %)	25.8 (−20.5 %)	28.1 (−22.3 %)	24.0 (−19.1 %)

sky conditions (see Tab. 6; FU Clear-Sky and FU Non-Clear-Sky), the contrast is clear and expected: the model reproduces SWin with high accuracy during clear-sky periods. This level of accuracy is not achieved in episodes with cloud cover, where performance metrics degrade noticeably for both variables. PALM’s overall performance shows that SWin is represented with high fidelity under clear-sky conditions when using the updated FU-driving data. Although PALM’s simulation of SWout is not poor, a clear deterioration in the evaluation metrics is evident, particularly at vegetated sites. Under conditions other than clear skies, PALM struggles to model radiation, and its performance remains inconsistent.

**Table 6.** Statistical performance metrics for PALM-simulated incoming (SWin) and outgoing (SWout) short-wave radiation across four measurement stations (FSV, NTK, HAN, and FLE). The upper part refers to the PALM outputs driven by the WRF-CNU and WRF-FU configurations during clear-sky conditions and common episodes, and the bottom section compares PALM outputs driven by the WRF-FU configuration during clear-sky and non-clear-sky episodes (see Table. 4). Metrics include Pearson correlation ( $r$ ), coefficient of determination ( $R^2$ ), Spearman's rho ( $\rho$ ), Kendall's tau ( $\tau$ ), and Willmott's index of agreement ( $d$ ). The formulas used for the statistical analysis are described in the supplementary material, under the metrics defined in Supplement Section 1.

Station	Variable	CNU Common Clear-Sky					FU Common Clear-Sky				
		$r$	$R^2$	Spearman's $\rho$	Kendall's $\tau$	$d$	$r$	$R^2$	Spearman's $\rho$	Kendall's $\tau$	$d$
<b>FSV</b>	SWin	0.993	0.922	0.992	0.934	0.980	0.987	0.966	0.989	0.932	0.992
	SWout	0.981	0.774	0.982	0.891	0.939	0.963	0.830	0.968	0.854	0.957
<b>NTK</b>	SWin	0.996	0.928	0.995	0.951	0.978	0.994	0.985	0.989	0.913	0.995
	SWout	0.992	0.842	0.979	0.889	0.955	0.990	0.941	0.973	0.874	0.985
<b>HAN</b>	SWin	0.983	0.939	0.976	0.867	0.987	0.981	0.963	0.979	0.882	0.994
	SWout	0.826	-1.332	0.866	0.685	0.625	0.730	-1.438	0.802	0.626	0.620
<b>FLE</b>	SWin	0.984	0.947	0.987	0.913	0.983	0.978	0.950	0.981	0.890	0.988
	SWout	0.982	0.909	0.980	0.880	0.963	0.970	0.913	0.973	0.856	0.977
<b>Overall</b>	SWin	0.989	0.934	0.988	0.916	0.982	0.985	0.966	0.984	0.904	0.992
	SWout	0.945	0.298	0.952	0.836	0.870	0.913	0.312	0.929	0.802	0.885
Station	Variable	FU Clear-Sky					FU Non-Clear-Sky				
		$r$	$R^2$	Spearman's $\rho$	Kendall's $\tau$	$d$	$r$	$R^2$	Spearman's $\rho$	Kendall's $\tau$	$d$
<b>FSV</b>	SWin	0.989	0.974	0.991	0.926	0.993	0.957	0.889	0.943	0.818	0.972
	SWout	0.971	0.847	0.976	0.860	0.955	0.950	0.859	0.904	0.742	0.960
<b>NTK</b>	SWin	0.993	0.980	0.989	0.909	0.994	0.886	0.676	0.900	0.733	0.904
	SWout	0.990	0.952	0.974	0.869	0.987	0.881	0.711	0.864	0.692	0.901
<b>HAN</b>	SWin	0.988	0.971	0.985	0.898	0.994	0.960	0.882	0.953	0.857	0.971
	SWout	0.493	-1.806	0.698	0.526	0.574	0.568	-0.804	0.625	0.450	0.604
<b>FLE</b>	SWin	0.973	0.944	0.982	0.893	0.986	0.938	0.872	0.847	0.667	0.967
	SWout	0.966	0.915	0.970	0.853	0.977	0.940	0.881	0.786	0.590	0.967
<b>Overall</b>	SWin	0.986	0.967	0.987	0.907	0.992	0.935	0.830	0.911	0.769	0.954
	SWout	0.855	0.227	0.904	0.777	0.873	0.935	0.412	0.795	0.618	0.858



Fig. 2 illustrates PALM performance and accuracy through the MBE and RMSE error distributions for both incoming and reflected short-wave radiation across four stations. The arrangement in Fig. 2 is to isolate the impact of driving data and reflected short-wave radiation across four stations. The arrangement in Fig. 2 is to isolate the impact of driving data  
270 configurations and sky conditions on the model's performance. In the CNU-driven setup, the incoming short-wave radiation (SWin-CNU) is underestimated across all evaluated stations. The negative biases span from  $-13 \text{ Wm}^{-2}$  to  $-46 \text{ Wm}^{-2}$ , most pronounced at the FSV and NTK stations (Fig. 2a). Conversely, for SWin-FU, the MBE values are significantly reduced, approaching 0, and at the HAN and FLE stations, they become slightly positive. For outgoing short-wave radiation, both SWout-CNU and SWout-FU exhibit negative biases, which are reduced when using the FU configuration. The only exception  
275 is the HAN station, where both setups show a strong negative bias greater than  $-30 \text{ Wm}^{-2}$ . This bias pattern is further supported by the RMSE values (Fig. 2d), which decrease for the FU configuration for both incoming and outgoing short-wave radiation, although the reduction is less pronounced for the outgoing component.

SWin-FU biases (Fig. 2b) display a site-specific performance pattern comparable to that in Fig. 2a, with negative biases at urban stations (FSV and NTK) and positive biases at vegetated stations (HAN and FLE). SWout MBEs are generally small,  
280 except for the pronounced negative bias at the HAN station ( $\approx -60 \text{ Wm}^{-2}$ ), which remains evident and aligns with earlier analyses. The RMSE values are generally moderate; however, for SWout at the HAN station, they are notably higher than at the other stations. Finally, under non-clear-sky conditions, the model performance degrades notably, as indicated by large MBE and RMSE values, particularly for SWin (Fig. 2c,d). In the case of SWin, MBEs indicate model overestimation, with the highest value exceeding  $120 \text{ Wm}^{-2}$  at the NTK station. SWout biases are negative, except for the NTK station, which has a  
285 positive bias.

To separate the effect of the driving model setup on the PALM-simulated short-wave radiation, we perform a direct, point-by-point comparison, as shown in Figure 3 and Figure 4. Firstly, in the CNU-driven PALM simulations, SWin is consistently and systematically underestimated for irradiance values exceeding  $600 \text{ Wm}^{-2}$  (see Fig. 3a). This deviation is evident in the relatively large MBE and RMSE values of  $-32.05 \text{ Wm}^{-2}$  and  $62.21 \text{ Wm}^{-2}$ , respectively. The consistent underestimation suggests  
290 that the deficiencies likely stem from the WRF-CNU driving setup and cannot be fully mitigated by PALM's high-resolution local radiative transfer calculations. In contrast, a clear improvement is observed for the WRF-FU-driven PALM simulations, in which the MBE is reduced by roughly one order of magnitude and the RMSE decreases by about 30 % compared to the CNU-driven PALM simulations (see Fig. 3b). However, the FU-based outputs at radiation levels below  $300 \text{ Wm}^{-2}$  show a slight spread around the 1:1 line. A noticeable deterioration in PALM's performance (also for the FU-based outputs) is evident for  
295 outgoing short-wave radiation, as illustrated in Figure 4. An initial assessment common to both configurations is a systematic underestimation of outgoing short-wave radiation, which is somewhat more pronounced when using the CNU driver. This underestimation results in a negative bias of  $-16.15 \text{ Wm}^{-2}$  for CNU and  $-12.61 \text{ Wm}^{-2}$  for the FU configuration, corresponding to an approximate reduction of 22 % in favour of the FU setup. As indicated by the RMSE values, PALM's predictions remain moderately accurate, though slightly improved in the FU configuration. Furthermore, the evaluated stations exhibit more variability for outgoing radiation. For instance, FLE (blue) and NTK (purple) align relatively well with the observations (Fig. 4b),  
300 whereas the HAN (green) station exhibits significant deviations and has the poorest correspondence (Fig. 4a,b). Although the results show that the FU driver reduces bias relative to the CNU, discrepancies with observations remain relatively high. It



implies that the model’s inadequate representation of surfaces near problematic sites (i.e., HAN) influences reflected radiation and is the primary cause of these biases.

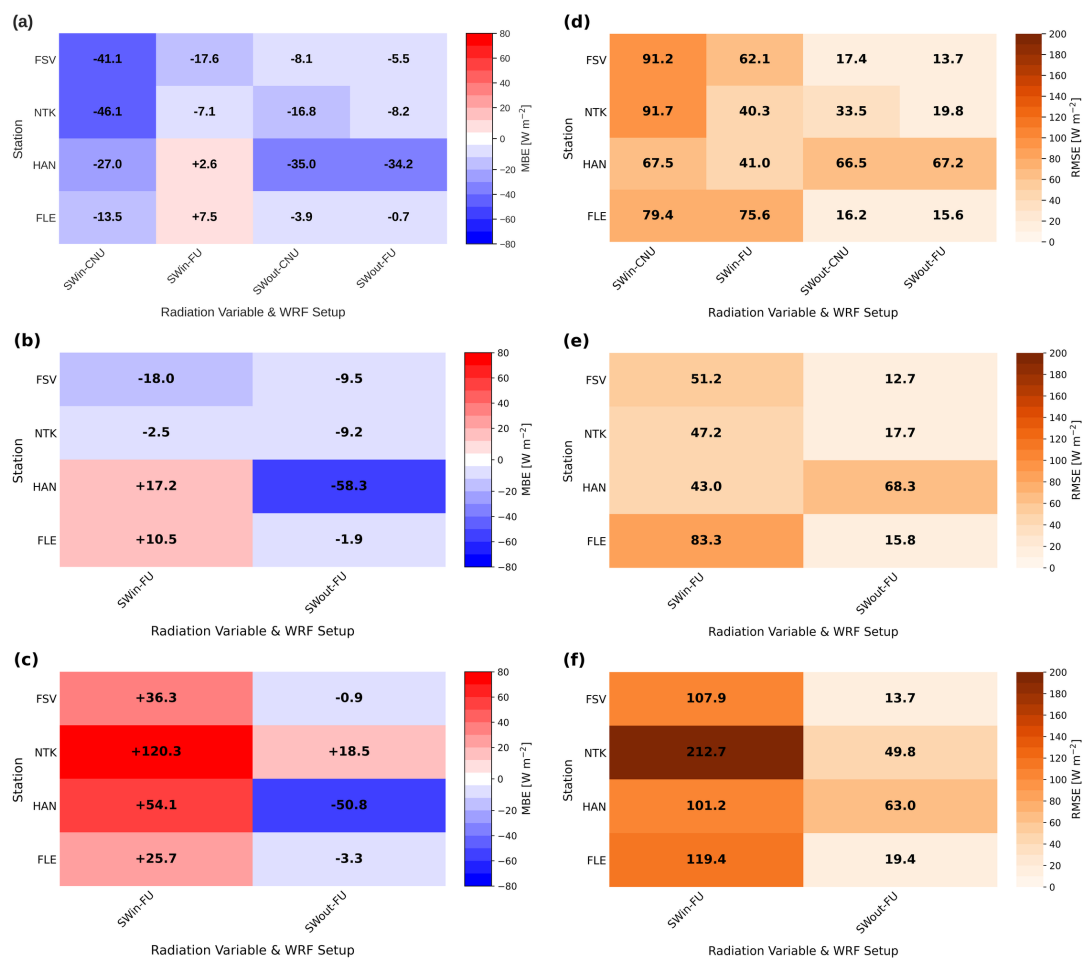


**Figure 2.** Summary Mean Bias Errors (MBE; a–c) and Root Mean Square Errors (RMSE; d–f) of short-wave incoming (SWin) and short-wave outgoing (SWout) radiation across 4 observational stations (FSV, NTK, HAN, and FLE) and different WRF driving data setups. Each cell contains the error averaged over the corresponding episode selection for a specific variable, observational station, and WRF model driving setup. Panels (a) and (d) correspond to the common simulated episodes driven by both CNU and FU WRF model setups, panels (b) and (e) refer to the clear-sky FU WRF model setup, while non-clear-sky episodes with the FU WRF model setup are depicted on panels (c) and (f). The colour bars represent the magnitude of the MBE and RMSE values in  $Wm^{-2}$ .

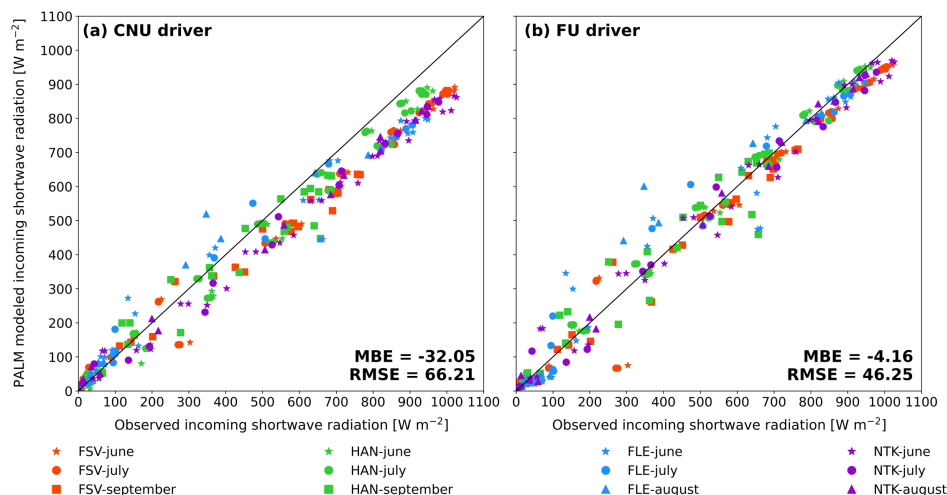


**Figure 3.** Scatter plots of incoming short-wave radiation for all common simulated episodes (e3, e5, e6, e8, e9, e16) and all measuring stations for the Coarse No Urban (CNU; a) and Fine Urban (FU; b) WRF-driving setup. Colours represent individual stations (FSV–red, HAN–green, FLE–blue, and NTK–purple) while marker shapes represent months of the simulated episodes (star–June, circle–July, triangle–August, and square–September). The summary Mean Bias Error (MBE) and Root Mean Square Error (RMSE) depict PALM’s performance compared with observations.

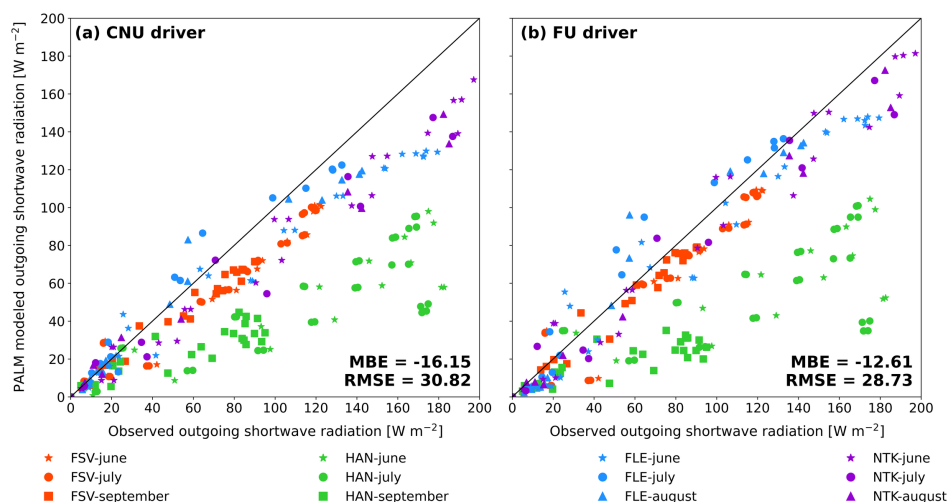


**Figure 4.** Scatter plots of outgoing short-wave radiation for all common simulated episodes (e3, e5, e6, e8, e9, e16) and all measuring stations for the Coarse No Urban (CNU; a) and Fine Urban (FU; b) WRF-driving setup. Colours represent individual stations (FSV–red, HAN–green, FLE–blue, and NTK–purple) while marker shapes represent months of the simulated episodes (star–June, circle–July, triangle–August, and square–September). The summary Mean Bias Error (MBE) and Root Mean Square Error (RMSE) depict PALM’s performance compared with observations.



## 305 3.2 Daily cycles of incoming and outgoing short-wave radiation

Addressing the main model outputs through diurnal cycles of incoming and outgoing short-wave radiation components is a well-established benchmark for testing the overall fidelity of micro-scale models. The significance of urban meteorology studies, in particular, is underscored by the ability to capture the relationship between the moving Sun and surrounding physical objects, radiation intensity, surface albedos, and the integration of dynamic driver data. Although significant, statistical summaries cannot fully capture the specifics of the model's radiative process treatment (e.g., resolving morning and afternoon shading patterns, midday radiation intensity offsets or magnitude discrepancies, location-specific sensitivities, surface-type biases). Hence, the following subsections are organised into three complementary evaluations that demonstrate the model's fidelity (Section 3.2.1), reveal instances where the performance bottlenecks are most clearly evident (Sections 3.2.2), and validate the model's predictive skills under more complex radiative regimes (Section 3.2.3).

### 315 3.2.1 PALM's fidelity in reproducing diurnal shading patterns

The ability to resolve shading patterns within a local urban environment is a key distinguishing feature of high-resolution models such as PALM, compared with coarser, less extensive meteorological models (e.g., meso-scale or diagnostic models). The direct effect of heterogeneous urban morphology (i.e., building, street canyon, and vegetation patterns) on incoming short-wave radiation is most apparent for small solar elevation angles during sunrise and sunset. As seen from the Fig. 5, the driving model's deficiencies are evident in its inability to accurately capture the shading effects imposed on incoming solar radiation during early morning and late afternoon, whereas PALM reproduces the observed SWin profile shape with high accuracy. One notable improvement occurs during maximum solar irradiance, when the FU-driven simulation fully reproduces the SWin amplitude. In contrast, the CNU-driven setup systematically underestimates the observed solar-noon peak. This enhancement is evident at the urban NTK station, where the FU-WRF simulation shows a deficit of about  $80\text{--}100\text{ W m}^{-2}$ , while the CNU-WRF simulation shows an even greater deficit relative to the observed values. The SWout is simulated reasonably well by both drivers, with a similar diurnal pattern of underestimating the reflected radiation throughout the day. Although the FU-driven SWout increases minimally throughout the day, it remains consistently higher than the CNU-driven simulation and matches more closely the observed values.

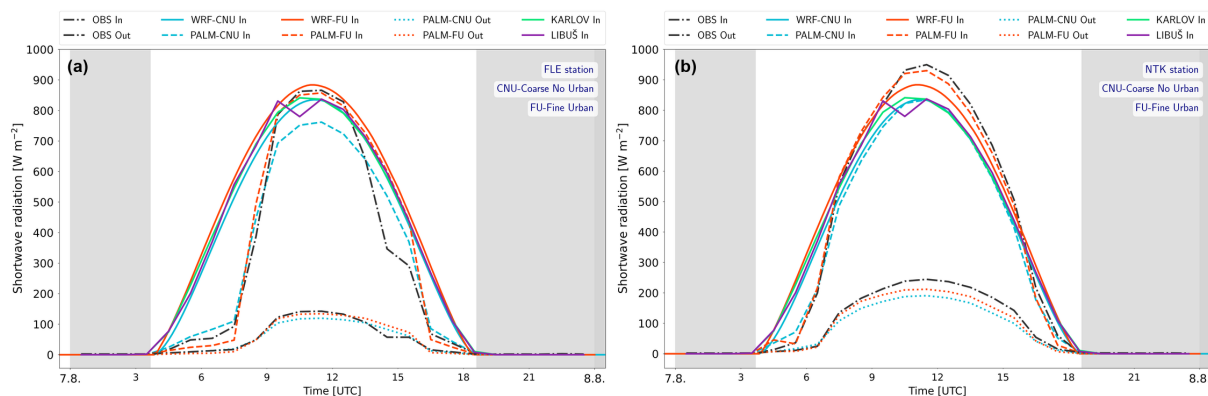


**Figure 5.** The comparison of observed hourly averages of incoming (In) and outgoing (Out) short-wave radiation for the e6 episode at the stations FLE (a) and NTK (b), with PALM model outputs for both WRF configurations. Additional lines represent the raw WRF outputs, Coarse No Urban (WRF-CNU), and Fine Urban (WRF-FU), and measurements from professional meteorological stations in Karlov and Libuš.

### 3.2.2 Vegetation effects and midday underestimation

330 Vegetation modulates both the incoming and outgoing short-wave radiation through processes such as absorption, reflection, and scattering. This effect is clearly captured during episode e5. As shown in Fig. 6a, the incorrectly parameterised grass cover in the PALM's static driver at the HAN station translated directly to the SWout data output by the micro-scale simulation for both WRF driving configurations. The influence of site-specific variability on SWout modelling is evident in the contrasting behaviour of PALM-simulated SWout at the urban FSV station, where both PALM setups reproduced in situ measurements, although the CNU-driven configuration performed slightly worse than the FU. During midday, the magnitude of the PALM-modelled reflected radiation drops below  $100 \text{ W m}^{-2}$ , which is inconsistent with observations that show values between 180 and  $200 \text{ W m}^{-2}$ . These qualitatively identified discrepancies in the SWout are evident in other analyses, where the HAN station shows the worst quantitative performance, as indicated by high MBE and RMSE values along with other supporting statistical indicators (see e.g., Figs. 2 and 4, or Tabs. 5 and 6). Another discrepancy of PALM is the midday underestimation of SWin

335

340 observed at the urban FSV station. Across both WRF forcing configurations, PALM underestimates the incoming short-wave radiation, although this offset is moderately attenuated by PALM-FU downscaling.

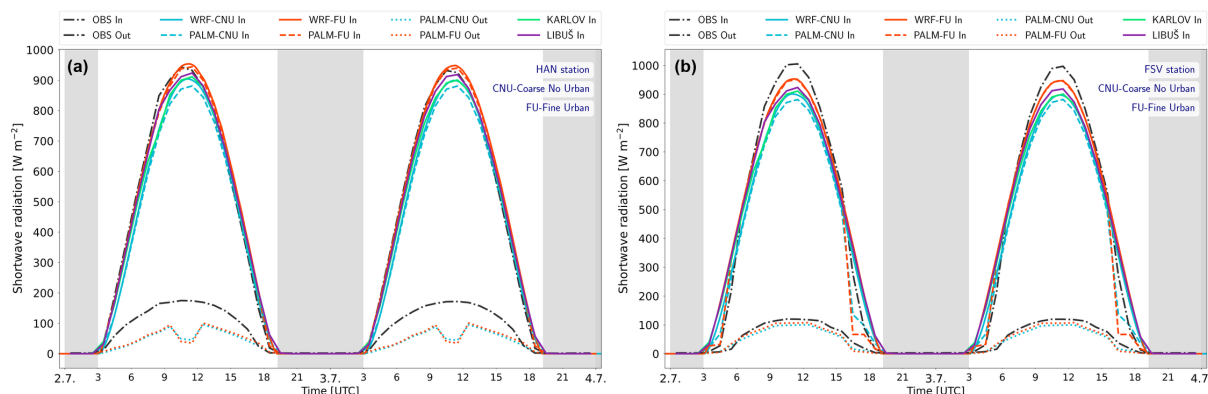


**Figure 6.** The comparison of observed hourly averages of incoming (In) and outgoing (Out) short-wave radiation for the e9 episode at the stations HAN (a) and FSV (b), with PALM model outputs for both WRF configurations. Additional lines represent the raw WRF outputs, Coarse No Urban (WRF-CNU), and Fine Urban (WRF-FU), and measurements from professional meteorological stations in Karlov and Libuš.

### 3.2.3 PALM’s performance during non-clear sky conditions

As a physical factor, clouds are complex regulators of short-wave radiation flux, affecting both its magnitude and timing. Hence, the shape of the incoming short-wave radiation function during periods of variable cloud cover deviates from its clear-sky counterpart, which is roughly symmetrical with its maximum around solar noon. Caused by physical and numerical factors, the resolution and modelling of short-wave radiation under non-clear-sky conditions pose a challenge for all types of meteorological models, regardless of spatial resolution. In this section, we evaluate PALM’s robustness in capturing radiation during non-idealised (i.e. non-clear-sky) cases through three selected episodes (e9, e10, and e12) characterised by cloudy or partly cloudy conditions (see Fig. 7). In the first analysed episode, e9, the advantages of PALM’s downscaling are most evident at the vegetated FLE station (see Fig. 7a). Up to around midday, PALM diverges from its driving data and adjusts the SWin profile toward the observed values. However, after noon, PALM no longer matches the observations and aligns more closely with its driving data. The SWout shows a more uniform pattern, with PALM aligning well with the observed outgoing radiation in the morning hours, underestimating it around noon, and slightly overestimating it in the afternoon. For the same episode and the urban NTK station, both SWin and SWout discrepancies are large. PALM does not align with the observed values and follows its driving data entirely. These deviations at the NTK station are clearly seen through the quantitative evaluations presented in Table 5 and Table 6, as well as in the MBE and RMSE errors in Fig. 2. For episodes e10 and e11 at the FSV station, during the early morning hours (i.e., 3–6 am), PALM corrects its driving data and aligns the SWin profile with the observations. However, during midday in episode e10 and in the afternoon of episode e12, where the effect of the clouds is pronounced the most (Fig. 7bcef), PALM’s downscaling cannot mitigate the incorrect information in the WRF data, which does not capture the clouds present at the Karlov and Libuš reference stations and at the observation sites. The identified underestimation of SWout at the HAN station also persists during the non-clear-sky conditions, as seen in Fig. 7bc. Both CNU and FU configurations



exhibit bell-shaped SWin evolution, but the FU shows significantly higher values during the noon peak, while the CNU remains well below the observed values.

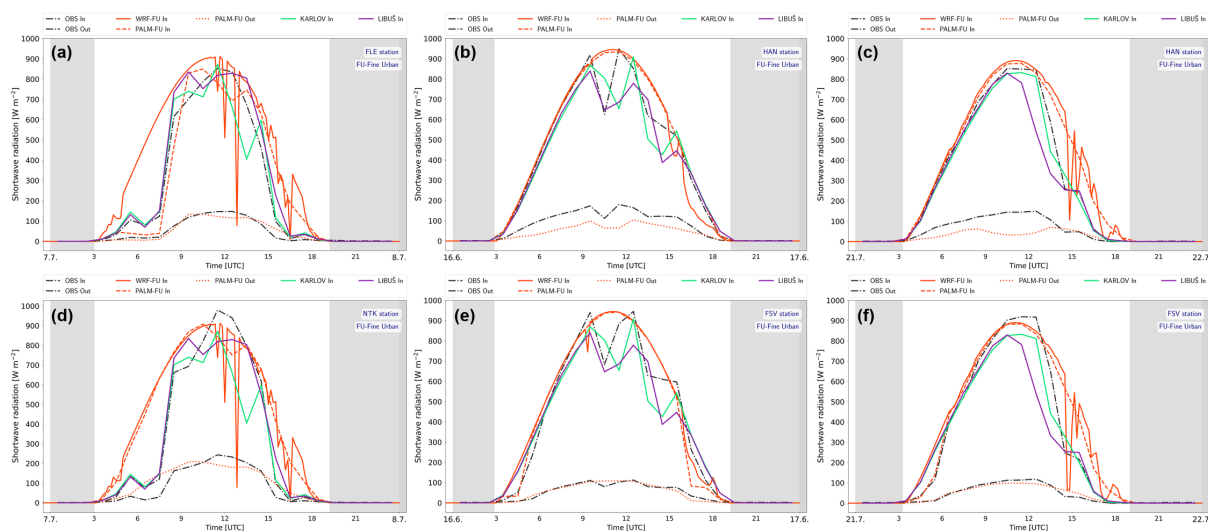


**Figure 7.** The comparison of observed hourly averages of incoming (In) and outgoing (Out) short-wave radiation during the non-clear sky episodes e9 (a,d), e10 (b,e), and e12 (c,f) at the selected station combinations, with PALM model outputs for both WRF configurations. Additional lines represent the raw WRF outputs, Coarse No Urban (WRF-CNU), and Fine Urban (WRF-FU), and measurements from professional meteorological stations in Karlov and Libuš.

## 4 Discussion

### 365 4.1 General model performance in simulating short-wave radiation

#### – Shadow patterns of urban morphology in modelling incoming short-wave radiation.

One of the key assets of PALM, identified in the study, is its ability to realistically simulate the magnitude of incoming short-wave radiation at morning and afternoon times as observed from street-level stations. Buildings, trees, and other obstacles cast the longest and broadest shadows during the hours when the Sun is near the horizon (i.e., early morning and late afternoon). Correctly reproducing the impact of urban obstructions (i.e., shadow patterns) on the detected SWin amount at the urban station requires explicitly integrating information on building and tree size, height, orientation, and spacing into the micro-scale model. At this point, the robustness of the RTM and PALM becomes evident: they can explicitly resolve sunlit and shaded surfaces and energy redistribution based on the calculated local sky view factors and shading geometry. Beyond their ability to resolve shading patterns, a further key aspect addressed by the micro-scale model is the correct translation of this information into short-wave flux magnitudes at the 1 m scale. Moreover, the visible delay and attenuated magnitude of the PALM-simulated SWin are corrected relative to the WRF driving



data, which most likely results from the WRF assuming unobstructed surfaces and therefore further overestimates  $SW_{in}$  during these hours.

380

However, certain disagreements between the micro-scale outputs and the observation data, resulting from incorrect urban canopy representation in the micro-scale model, are also identified (see Fig. 8 FLE station around 15:00 UTC, for example, PALM’s tree height is shorter than the real one, and  $SW_{in}$  is not attenuated enough, and Fig. S12 NTK around 04:00 UTC, where the tree is not represented accurately in PALM as well). As said, incident short-wave radiation is highly sensitive to the placement and dimensions of urban obstacles, so even small inaccuracies in the PALM static driver data can produce excess attenuation or an increase in the incoming radiation in the PALM’s outputs.

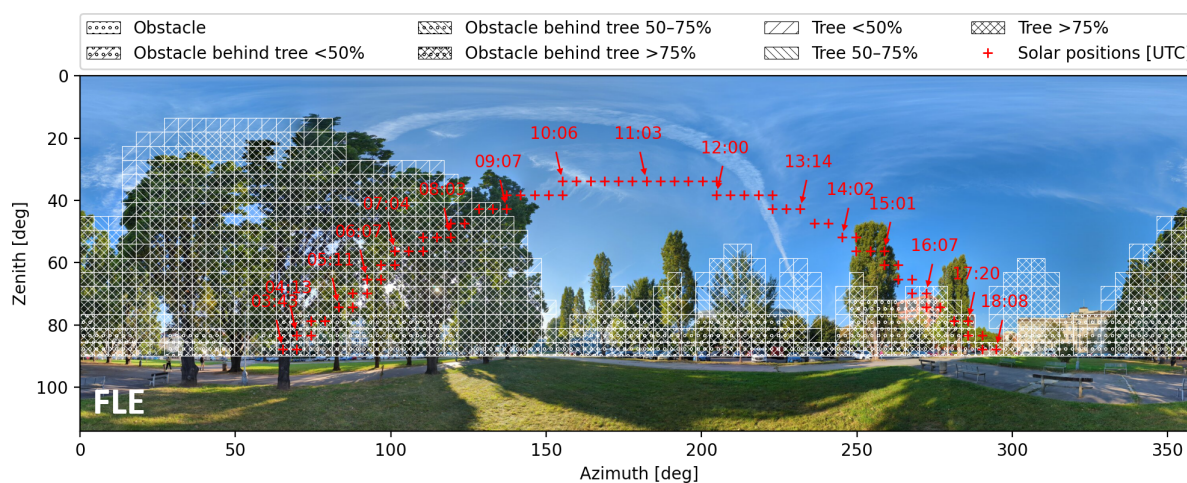


**Figure 8.** Hemispherical view at the FLE observation site with obstructions and vegetation as modelled by PALM, plotted in azimuth–zenith coordinates. Trees and obstacles are classified according to their fractional area coverage. Red crosses indicate the Sun’s trajectory throughout the day, with annotated timestamps in UTC.

385

– **PALM’s simulation of outgoing short-wave radiation.**

While the PALM model can simulate incoming short-wave radiation with a high degree of reliability at the 1 m scale, the outgoing short-wave radiation outputs indicate that modelling this variable poses a greater challenge for PALM and requires a more precise description of urban surface properties. The incoming short-wave radiation modelling is generally less challenging, as it is primarily governed by atmospheric transmissivity (e.g., cloud and aerosol presence) and the Sun’s position in the sky. In contrast, outgoing short-wave radiation is heavily influenced by the three-dimensional urban form, surface albedo, complex multiple reflections within urban canyons, and the structure of the vegetation canopy.

390

The general settings of surface albedo for vegetation in the static driver proved to be a significant source of bias in PALM’s modelling of reflected radiation. A good illustration supporting this statement is the HAN station, whose surroundings are rich in vegetation and covered by grassland. As seen from the daily  $SW_{out}$  profiles in Fig. 6, there is a significant reduction in the PALM modelled  $SW_{out}$  during the midday hours. Such a drop in the  $SW_{out}$  indicates low

395



400

reflection at this location, and consequently strong absorption, implying that PALM represents this area with low-to-moderate albedo values (indeed, the prescribed albedo for HAN in PALM is 0.17). It appears that the PALM is unable to capture variability in grassy surfaces; the only option is a manual setup for individual episodes. In reality, the grass moving at this location was not, most likely, periodic, as the measured SWout signal indicates more reflection and weaker absorption. The reflection could also be affected by available soil moisture, which varies daily and seasonally and is typically not accurately captured by WRF. The negative bias at the HAN station could not be mitigated, even with the improved WRF-FU setup, since the underestimation of the SWout at HAN stayed significant (e.g., see Fig. 4).

405

A notable tendency of the PALM model is a systematic underestimation of SWout, suggesting an excessive sink of short-wave radiation (i.e., pronounced negative MBE values, see Fig. 2a–c). These negative biases are attributable to the inaccurately represented vegetation, prescribed albedo, and geometric factors, rather than to biases in the meso-scale driving data or in the WRF model setup. This behaviour does not inherently imply poor performance of the micro-scale model; instead, it reflects the challenge of accurately simulating outgoing short-wave radiation in highly heterogeneous, densely built urban environments. Although the SWout magnitude is generally underestimated, PALM simulates its temporal evolution and variability very well, as evidenced by strong overall correlations (see Tab. 6). Furthermore, the scale of the MBE at the FSV, NTK, and FLE stations is generally smaller (despite the remaining underestimation), directly demonstrating PALM’s capability to accurately assess reflections from complex urban geometry, canyon shading effects, and to provide sufficiently precise albedo values and urban surface properties.

410

- **Underprediction of the incident short-wave radiation at solar noon:** The systematic SWin underestimation at the evaluated stations around solar noon during the clear-sky episodes (mainly in the WRF-CNU setup) results from a “chain reaction” originating from the WRF’s driving data supplied to PALM. PALM’s modelling independence during this period is clearly limited, as it either amplifies or maintains the same level of bias in its outputs without imposing significant corrections, and it does not reach the peak intensity measured at the observation site. In principle, during clear-sky conditions at solar noon, the systematic underestimation of SWin is unlikely to be solely attributable to shadings induced by urban structures. At this time of day, the Sun’s zenith angle is low, and the incoming short-wave radiation travels nearly vertically. It minimises any geometry-induced shading or surface-based effects, suggesting that the SWin underestimation is most likely driven by other factors (e.g., the SWin definition before reaching the canopy height and the observation point within the micro-scale model domain).

415

420

425

The distinction between both WRF configurations’ solar-noon performance reinforces the above argument; the WRF-FU configuration significantly reduces the solar-noon discrepancies that are clearly observed in the WRF-CNU runs (see e.g., Supplement Fig. S2). This suggests that the short-wave radiation inherited from the WRF-CNU driving data is the primary source of PALM’s systematic noon bias. The PALM internal factors (e.g., RTM, USM, PCM, static driver data) play only a secondary role or may have no effect. Within the WRF model framework, several factors can lead to excessive underestimation. First, inaccuracies in WRF’s driving data (i.e., ERA5) may introduce an overestimated amount of aerosols or water vapour concentrations in WRF simulations and bias its radiative calculations. Second, WRF’s radiation



430 scheme can itself overestimate the absorption and scattering by aerosols, water vapour or other atmospheric constituents  
within the WRF domain, and consequently overestimate the absorption and scattering of the actual amount of short-wave  
radiation. Alternatively, physical parameterisation in WRF's PBL schemes could lead to weak vertical mixing and trap  
moisture in the lower layers, further attenuating the magnitude of short-wave radiation. The PALM model inherits the  
bias and starts its simulations with reduced top-of-domain downwelling short-wave radiation. Since the SWin PALM's  
435 output magnitude is reduced relative to observations (and, in certain cases, even lower than its WRF driving data), the  
loss of the SWin magnitude between the top of PALM's domain and the sensor grid point could be caused by incorrectly  
modelled surface-sky radiative interactions. Potential error could lie in incorrect redistribution or underestimation of  
diffuse short-wave radiation within PALM's surface, canopy, and geometry-related routines. However, although PALM's  
internal modules can affect SWin underestimation, their influence is secondary to that of WRF.

#### 440 4.2 Driving data impact: WRF-CNU vs. WRF-FU configuration performance

A primary outcome of the driving-data impact evaluation on micro-scale simulations is the added value of the FU and the  
lower accuracy of the CNU configuration for PALM micro-scale simulations. Although both setups reproduced temporal SWin  
evolution well relative to the observed values (with FU being more accurate), differences between them are reflected in the  
magnitude of bias and in overall statistical metrics of the evaluated PALM outputs.

445 The central differences between the two WRF setups are in their horizontal resolutions and physics parameterisation bundles  
as presented in Table 1. The CNU configuration does not include information on urban canopy, geometry, or three-dimensional  
objects (i.e., buildings) and has a coarser 3 km resolution. A combination of these WRF-CNU features produces smoother  
radiation fields and overestimates morning and late-afternoon incoming SW radiation by failing to account for urban physical  
structures and shadowing effects. The inability to represent building-involved shadowing effects is evident in the qualitative  
450 analysis, e.g., Fig. 5, where the WRF-CNU setup predicts an earlier and accelerated morning increase, as well as a delayed  
afternoon reduction in SW incoming radiation compared to the observation.

The improved resolution and more explicit treatment of urban morphology in the FU configuration benefit the FU-driven  
PALM simulation outputs. This is evidenced by improved overall statistical metrics (i.e., reduced MBE and RMSE and higher  
agreement metrics) and a lower difference between peak solar noon insolation and observations. Even though the WRF-FU  
455 setup's departure from observation in SWin is evident in morning and afternoon street-level shadowing patterns, its midday  
maxima are more realistic, and this configuration demonstrates a higher degree of agreement with observations from both  
CHMU and dedicated measurement stations. Finally, the FU's overall superiority is seen in reduced dispersion of PALM's  
SWin and SWout values (see Fig. 3 and Fig. 4).

Given these findings, the WRF-CNU driving dataset impairs PALM's performance due to biased radiation input fields,  
460 whereas the WRF-FU setup provides PALM with more accurate radiation fields. As previously demonstrated in Radović et al.  
(2024) and Resler et al. (2024) for meteorological variables (i.e., temperature and wind speed), this study emphasises both the  
importance of highly accurate radiation input fields and PALM's sensitivity to the quality of meso-scale radiation forcing. Since



PALM's and the RTM's limited capability to simulate complex radiative transfer processes is insufficient to correct biases in the driving fields, supplying the micro-scale model with realistic and robust meso-scale radiation forcing is imperative.

#### 465 **4.3 The effects of sky conditions on micro-scale simulations**

Undoubtedly, this study demonstrates clear performance degradation of the micro-scale model under non-clear-sky conditions relative to the clear-sky conditions, where PALM's RTM exhibits high-quality performance. During clear-sky conditions, the Sun's position relative to the Earth and the city's structure predominantly control the radiation field. In such cases, PALM's RTM modelling, with meter-scale resolution, explicitly resolves the detailed processes that affect radiation fluxes and accurately simulates the spatio-temporal dynamics of incoming short-wave radiation (i.e., exhibiting high temporal coherence with observations, good magnitude and phase alignment, and strong statistical performance). When the variability in incoming radiative fluxes is caused by intermittent cloud cover, PALM's framework is unable to capture rapid spatiotemporal fluctuations in radiative fluxes because it depends on information from the meso-scale model. The performance degradation is more pronounced in PALM's SWin outputs, as evidenced by overestimated incoming radiation, low correlation, and generally poor statistical performance. PALM's ability to accurately capture and redistribute radiation based on finely detailed, high-resolution geometry is insufficient for capturing the effects of cloud pattern shifts. Under cloud-cover conditions, the PALM is driven by the input conditions given by WRF. Temporal mismatches in cloud passages lead to large discrepancies in radiation values, thereby further reducing correlation and increasing relative errors. However, it is important to keep in mind that PALM's limited fidelity under non-clear-sky conditions does not represent a failure of the model itself and that its predictive skill remains reasonably good.

#### 475 **4.4 The importance of accurate short-wave radiation modelling for urban climate research and climate change adaptation and mitigation**

Short-wave radiative fluxes play a critical role in urban surface energy balance and strongly control urban climate, thermal comfort, and energy consumption in urbanised areas. If they are not captured accurately, errors and uncertainties in the radiative fluxes computed by PALM's RTM will propagate through the rest of the model framework and, in turn, affect all other variables that depend on them, thereby diminishing the overall reliability of the simulation. Establishing reliable simulations is especially important when the micro-scale model is applied to human biometeorological studies or to the development of urban adaptation or mitigation scenarios.

In human biometeorology, particularly in cities, SWin and SWout are crucial for estimating the thermal exposure and evaluating human thermal comfort. In essence, these two variables govern the MRT, the most important variable for calculating thermal comfort indices such as UTCI and PET. The incoming short-wave radiation determines the level of solar exposure within cities (e.g., in sunlit areas such as open squares, wide streets, large public squares and plazas, and similar spaces). In contrast, reflected short-wave radiation contributes to the amount of radiative load imposed by buildings, roads, and surrounding surfaces on urban dwellers. Inaccurate calculations of these radiative variables can lead to misidentification and mapping



495 of heat-vulnerable locations within cities, as well as to incorrect assessments of both the magnitude and the spatial distribution of heat stress.

From an application perspective, precise short-wave flux calculations are crucial for urban planning and design purposes, as well as for the development of mitigation strategies. Since the amount of SWin cannot be controlled, its precise and high-resolution modelling is fundamental to urban planning and design; without it, the strategic arrangement and optimisation of building orientation and placement, street layouts, shade sail installation, and tree positioning would be less effective. In certain situations, inappropriate mitigations may fail, leading to increased heat stress, distorted heating and cooling loads, and reduced overall urban sustainability. On the other hand, the SWout is a variable that urban planners can “control” to a certain extent, as it can be altered by choosing urban materials that, for example, promote cooling. Our results emphasise the high sensitivity of the SWout to the input static driver data. Hence, effectively simulating any pavement-based mitigation strategy or evaluating pavement albedos requires both reliable urban static driver datasets and fidelity in PALM’s SWout calculation procedures. Only if these two conditions are met can the predicted benefits and drawbacks of a designed strategy be considered realistic and applicable to urban sustainability planning (e.g., urban heat mitigation, thermal comfort improvements, and the long-term resilience of cities).

#### 4.5 Limitations and future aspects

510 – **Static driver data accuracy constraints:** Despite substantial efforts to ensure data quality (see section 3.2 in Resler et al., 2021), PALM’s static driver dataset is inherently prone to inaccuracies in urban morphology, land cover, and vegetation characteristics. This makes it a weak link in the micro-scale simulation framework and a major source of internally driven uncertainty, because it is practically impossible to map and keep all urban surfaces up to date. Due to the high heterogeneity of urban elements within the micro-scale simulation domain, uncertainties can arise from any component defined in the static dataset (Belda et al., 2021). They can lead to systematic errors that directly affect both SWin and SWout. Static driver data that may be erroneous includes, for example, building height and location, roof geometry, surface material, surface optical properties (e.g., albedo), vegetation height and spatial placement, and leaf area density. Spherical photography at the measurement location can be used to identify these discrepancies as potential sources of errors, as shown in Figure 8.

520 Simplified or idealised albedos and their deviations from actual “real-world” values for roofs, walls, pavements, and vegetated surfaces are the main contributors to incorrect estimates of reflected radiation (as illustrated at the HAN station). In addition, these incorrectly represented albedos also affect the final value of the modelled SWin, owing to the multiple-reflection processes represented and permitted by PALM’s RTM. In reality, urban objects, surfaces and vegetation are not “static” – they are prone to change due to ageing, season, and temporary or permanent human modification. Since such limitations inevitably reduce simulation accuracy, future work should prioritise continuous updates to urban morphology datasets and their utilisation in micro-scale models, such as PALM.



- 530
- **Limitations imposed by the meso-scale driving data:** PALM’s modelling freedom is limited by its dependence on the meso-scale driving data, as demonstrated throughout this work. The meso-scale errors propagate to micro-scale simulations, introducing significant biases in PALM’s radiation-dependent variables and outputs. Therefore, future studies should focus on improving the accuracy of cloud development, transfer, and optical properties within the meso-scale model, and on assessing its reliability prior to conducting simulations. This would significantly strengthen confidence in PALM’s applicability under non-clear-sky conditions and further enhance the fidelity of its simulations, even when it already performs well under clear-sky conditions. From an objective standpoint, future studies should focus on developing and refining more sophisticated coupling strategies for meso-scale and micro-scale models.
- 535
- **Observational limitations:** Our validation is not supported by a dense observation network but is performed against four point-based measurement locations that cover only a limited spatial area. Consequently, this study is inherently constrained by a limited spatial sampling and may not fully reflect PALM’s fidelity in capturing radiation variability within the simulated domain. Future efforts should prioritise establishing a denser and more heterogeneous observational network to enable a more comprehensive evaluation of the micro-scale model.
- 540
- **Transferability and representativeness of the results:** This analysis presents a case study of a unique urban configuration in Prague that encompasses both densely built-up areas and vegetation-covered environments. Hence, the validation and performance evaluation of PALM’s RTM remain specific to this context; applying the modelling framework to a different city or urban environment may reveal limitations not captured within the simulation domain used in this study. Furthermore, this study assesses only a limited number of episodes during the summers of 2017 and 2018. Conclusions drawn from this ensemble of episodes may not be transferable to other seasons, even though these episodes were
- 545
- deliberately selected for their relevance to, e.g., urban heat stress.

## 5 Conclusions

The central objective of this study is to examine the ability of the micro-scale model PALM to simulate both incoming and outgoing short-wave radiation in a densely built urban environment. Following that, the experiment investigates how structurally complex urban morphology and vegetation modulate these radiative fluxes and exposes the uncertainties arising from meso-scale driving conditions and their effects on the micro-scale simulation. This was achieved by validating the micro-scale simulations against observed incoming and reflected radiation at four locations, each with different urban morphological properties, under various atmospheric cloud coverages. The PALM simulations are driven by two differently configured sets of boundary conditions from the meso-scale model WRF. Next, both qualitative and quantitative analyses of PALM-modelled radiative exchanges between buildings, pavements, and vegetation, as well as an evaluation of the uncertainties introduced by the driving data, are performed. In conclusion, the performed experiment has led to the following findings:

550

555

- The validation results showed the high fidelity of the micro-scale model in resolving the spatial and temporal variability of short-wave radiation in a radiatively complex, morphologically heterogeneous urban environment. The model is par-



560 ticularly robust in accounting for shading effects from buildings, treating multiple reflections within urban canyons, and  
vegetation-induced attenuation of short-wave radiation.

– From the PALM simulations, it is particularly noticeable how morphology and vegetation strongly influence the distri-  
bution of short-wave radiation at the one-meter scale. From a micro-scale modelling perspective, accurate reproduction  
of morning and evening shading patterns validates both the model’s physical consistency in representing urban radia-  
565 tive processes and the correct implementation of the urban static driver dataset within the model’s framework. On the  
other hand, this alteration of both incoming and reflected radiation is not resolved in coarser models like WRF. Hence,  
because PALM realistically reflects the spatial and morphological heterogeneity of the urban environment and improves  
the representation and calculation of urban radiative processes, it can be considered a reliable tool for urban climate  
assessment.

– The reliability of the high-resolution micro-scale model simulations is especially dependent on the quality of the driving  
570 data and the prescribed urban static driver dataset. Moreover, as an important outcome, we highlight that realistically  
represented downwelling radiation from the meso-scale model and the boundary conditions are indispensable for ob-  
taining reliable results from PALM’s high-resolution modelling framework. If the imposed meso-scale driving data does  
not reflect actual radiative and meteorological weather conditions and contains errors, the micro-scale model will inherit  
these inaccuracies, thereby constraining the reliability of its simulations. To manage this complex and significant issue,  
575 both meso-scale downwelling radiation and boundary conditions must be rigorously verified. Without prior examination  
of the driving data and the attribution of potential discrepancies, any interpretation of the micro-scale outputs remains  
restricted and unreliable.

– Building on the previous argument, the simulated cloud cover in the meso-scale model stands out as the most important  
physical driver and an essential source of potential uncertainty, because even the small inaccuracies in their representation  
580 can produce large deviations in downwelling short-wave radiation supplied to the micro-scale model. Therefore, future  
research should focus on improving the accuracy of cloud representation and cloud-related parameters in the driving  
data. This could be achieved using ceilometer measurements, all-sky imaging systems, satellite-derived cloud datasets,  
or machine-learning-based cloud reconstruction methods. Fine-tuned cloud depiction would substantially improve the  
coherence between real atmospheric conditions and meso-scale forcings, as well as between the meso-scale forcings  
585 and micro-scale simulations. Consequently, existing and potential biases could be removed from the meso-scale forcing,  
preventing further error propagation into the micro-scale simulation.

As a micro-scale model, PALM robustly simulates the radiative transfer of short-wave radiation as it propagates and interacts  
with the city’s complex geometry; however, the consistency of its output ultimately depends on the quality and accuracy of the  
prescribed static datasets and the meso-scale input forcing data. Finally, the experiment underscores that achieving PALM’s  
590 high-level predictive skill and generating reliable, climate-sensitive urban resilience strategies require prior examination of the  
driving datasets, along with methodical diagnostics and quantification of their underlying biases.



*Code and data availability.* The utilised source code, the PALM installation and usage guide description, the PALM model input data, the WRF model configuration files, and the observational datasets used for validation are stored at: <https://doi.org/10.5281/zenodo.19231961> (Radović et al., 2026).

595 *Author contributions.* J. Radović: Conceptualisation, Data curation, Formal analysis, Investigation, Methodology, Software, Supervision, Validation, Visualisation, Writing – original draft, Writing - Review & Editing. M. Belda: Formal analysis, Investigation, Writing - Review & Editing. M. Bureš: Data curation, Software, Validation, Visualisation. K. Eben: Software, Validation. Writing – review & editing. J. Geletič: Conceptualisation, Data curation, Formal analysis, Investigation, Methodology, Software, Supervision, Validation, Visualisation, Writing – original draft, Writing – review & editing. J. Jura: Data curation. P. Krč: Funding acquisition, Project administration, Data curation, Formal analysis, Software, Validation, Visualisation, Writing – review & editing. H. Řezníček: Writing – review & editing. J. Resler: 600 Conceptualisation, Funding acquisition, Project administration, Supervision, Software, Validation, Writing – review and editing.

*Competing interests.* The authors declare that they have no conflict of interest.

*Acknowledgements.* This work was supported by the Johannes Amos Comenius Programme (P JAC) project No. CZ.02.01.01/00/22\_008/0004605, Natural and anthropogenic georisks, by the MICROBUS project, which is financed from the state budget by the Technology Agency of the 605 Czech Republic and the Ministry of the Environment within the "Prostředí pro život 2" Programme, by the project Strategy AV21 Dynamic Planet Earth. The PALM simulations were performed on the HPC infrastructure of the IT4I supercomputing center supported by the Ministry of Education, Youth and Sports of the Czech Republic through the e-INFRA CZ (ID no. 90254). The WRF simulations, as well as pre- and postprocessing, were conducted on the HPC infrastructure of the Institute of Computer Science (ICS) of the Czech Academy of Sciences supported by the long-term strategic development financing of the ICS (RVO 67985807). The authors utilised Grammarly for grammatical 610 verification and to refine the scientific text throughout the drafting process.



## References

- Aminipouri, M., Knudby, A. J., Krayenhoff, E. S., Zickfeld, K., and Middel, A.: Modelling the impact of increased street tree cover on mean radiant temperature across Vancouver's local climate zones, *Urban Forestry & Urban Greening*, 39, 9–17, <https://doi.org/10.1016/j.ufug.2019.01.016>, 2019.
- 615 Aoyagi, T. and Takahashi, S.: Development of an Urban Multilayer Radiation Scheme and Its Application to the Urban Surface Warming Potential, *Boundary-Layer Meteorology*, 142, 305–328, <https://doi.org/10.1007/s10546-011-9679-0>, 2012.
- Baklanov, A., Grimmond, C. S. B., Carlson, D., Terblanche, D., Tang, X., Bouchet, V., Lee, B., Langendijk, G., Kolli, R. K., and Hovsepyan, A.: From urban meteorology, climate and environment research to integrated city services, *Urban Climate*, 23, 330–341, <https://doi.org/10.1016/j.uclim.2017.05.004>, 2018.
- 620 Belda, M., Resler, J., Geletič, J., Krč, P., Maronga, B., Sühling, M., Kurppa, M., Kanani-Sühling, F., Fuka, V., Eben, K., et al.: Sensitivity analysis of the PALM model system 6.0 in the urban environment, *Geoscientific Model Development*, 14, 4443–4464, <https://doi.org/10.5194/gmd-14-4443-2021>, 2021.
- Blocken, B.: Computational Fluid Dynamics for urban physics: Importance, scales, possibilities, limitations and ten tips and tricks towards accurate and reliable simulations, *Building and Environment*, 91, 219–245, <https://doi.org/10.1016/j.buildenv.2015.02.015>, 2015.
- 625 Blocken, B.: LES over RANS in building simulation for outdoor and indoor applications: A foregone conclusion?, *Building Simulation*, 11, 821–870, <https://doi.org/10.1007/s12273-018-0459-3>, 2018.
- Bougeault, P. and Lacarrere, P.: Parameterization of Orography-Induced Turbulence in a Mesobeta–Scale Model, *Monthly Weather Review*, 117, 1872 – 1890, [https://doi.org/10.1175/1520-0493\(1989\)117<1872:POOITI>2.0.CO;2](https://doi.org/10.1175/1520-0493(1989)117<1872:POOITI>2.0.CO;2), 1989.
- Bruse, M., Simon, H., and Sinsel, T.: Development and implementation of a high-resolution dynamical wall and roof model for ENVI-met. Part 1: General model design and non-vegetated walls and roofs, <https://doi.org/10.13140/RG.2.2.29309.95207>, [cited 8.10.2025], 2023a.
- 630 Bruse, M., Simon, H., and Sinsel, T.: Development and implementation of a high-resolution dynamical wall and roof model for ENVI-met. Part 2: Vegetated walls and roofs, <https://doi.org/10.13140/RG.2.2.36020.83842>, [cited 8.10.2025], 2023b.
- Chen, L., Yu, B., Yang, F., and Mayer, H.: Intra-urban differences of mean radiant temperature in different urban settings in Shanghai and implications for heat stress under heat waves: A GIS-based approach, *Energy and Buildings*, 130, 829–842, <https://doi.org/10.1016/j.enbuild.2016.09.014>, 2016.
- 635 Chen, T., Pan, H., Lu, M., Hang, J., Lam, C. K. C., Yuan, C., and Pearlmutter, D.: Effects of tree plantings and aspect ratios on pedestrian visual and thermal comfort using scaled outdoor experiments, *Science of the Total Environment*, 801, 149527, <https://doi.org/10.1016/j.scitotenv.2021.149527>, 2021.
- Clough, S., Shephard, M., Mlawer, E., Delamere, J., Iacono, M., Cady-Pereira, K., Boukabara, S., and Brown, P.: Atmospheric radiative transfer modeling: a summary of the AER codes, *Journal of Quantitative Spectroscopy and Radiative Transfer*, 91, 233–244, <https://doi.org/10.1016/j.jqsrt.2004.05.058>, 2005.
- 640 Dirksen, M., Ronda, R., Theeuwes, N., and Pagani, G.: Sky view factor calculations and its application in urban heat island studies, *Urban Climate*, 30, 100498, <https://doi.org/10.1016/j.uclim.2019.100498>, 2019.
- Dudhia, J.: Numerical study of convection observed during the winter monsoon experiment using a mesoscale two-dimensional model, *Journal of the Atmospheric Sciences*, 46, 3077–3107, <https://doi.org/10.1016/j.uclim.2019.100498>, 1989.
- 645 Fanger, P. O.: Calculation of thermal comfort: Introduction of a basic comfort equation, *ASHRAE Transactions*, 73, III4.1–III4.20, 1967.



- Freitas, S., Catita, C., Redweik, P., and Brito, M. C.: Modelling solar potential in the urban environment: State-of-the-art review, *Renewable and Sustainable Energy Reviews*, 41, 915–931, <https://doi.org/10.1016/j.rser.2014.08.060>, 2015.
- Fröhlich, D. and Matzarakis, A.: Spatial Estimation of Thermal Indices in Urban Areas—Basics of the SkyHelios Model, *Atmosphere*, 9, 209, <https://doi.org/10.3390/atmos9060209>, 2018.
- 650 Fröhlich, D., Gangwisch, M., and Matzarakis, A.: Effect of radiation and wind on thermal comfort in urban environments - Application of the RayMan and SkyHelios model, *Urban Climate*, 27, 1–7, <https://doi.org/10.1016/j.uclim.2018.10.006>, 2019.
- Gehrke, K. F., Sühling, M., and Maronga, B.: Modeling of land–surface interactions in the PALM model system 6.0: land surface model description, first evaluation, and sensitivity to model parameters, *Geoscientific Model Development*, 14, 5307–5329, <https://doi.org/10.5194/gmd-14-5307-2021>, 2021.
- 655 Geletiĉ, J., Lehnert, M., Resler, J., Krĉ, P., Middel, A., Krayenhoff, E., and Krüger, E.: High-fidelity simulation of the effects of street trees, green roofs and green walls on the distribution of thermal exposure in Prague-Dejvice, *Building and Environment*, 223, 109484, <https://doi.org/10.1016/j.buildenv.2022.109484>, 2022.
- Geletiĉ, J., Lehnert, M., Resler, J., Krĉ, P., Bureš, M., Urban, A., and Krayenhoff, E.: Heat exposure variations and mitigation in a densely populated neighborhood during a hot day: Towards a people-oriented approach to urban climate management, *Building and Environment*, 242, 110564, <https://doi.org/10.1016/j.buildenv.2023.110564>, 2023.
- 660 Geletiĉ, J., Lehnert, M., Krĉ, P., Resler, J., and Krayenhoff, E.: High-Resolution Modelling of Thermal Exposure during a Hot Spell: A Case Study Using PALM-4U in Prague, Czech Republic, *Atmosphere*, 12, 175, <https://doi.org/10.3390/atmos12020175>, 2021.
- Grylls, T. and van Reeuwijk, M.: How trees affect urban air quality: It depends on the source, *Atmospheric Environment*, 290, 119275, <https://doi.org/10.1016/j.atmosenv.2022.119275>, 2022.
- 665 Gál, C. V. and Kántor, N.: Modeling mean radiant temperature in outdoor spaces, A comparative numerical simulation and validation study, *Urban Climate*, 32, 100571, <https://doi.org/10.1016/j.uclim.2019.100571>, 2020.
- Hogan, R. J. and Bozzo, A.: A Flexible and Efficient Radiation Scheme for the ECMWF Model, *Journal of Advances in Modeling Earth Systems*, 10, 1990–2008, <https://doi.org/10.1029/2018MS001364>, 2018.
- 670 Holtanová, E., Belda, M., Randriatsara, H. H.-R. H., Szabó, A. I., and Halenka, T.: Scenarios of Köppen-Trewartha climate types in Europe based on GCM-RCM combined projections, *Theoretical and Applied Climatology*, 156, <https://doi.org/10.1007/s00704-025-05806-3>, 2025.
- Höppe, P. R.: The physiological equivalent temperature – a universal index for the biometeorological assessment of the thermal environment, *International Journal of Biometeorology*, 43, 71–75, <https://doi.org/10.1007/s004840050118>, 1999.
- 675 Iacono, M. J., Delamere, J. S., Mlawer, E. J., Shephard, M. W., Clough, S. A., and Collins, W. D.: Radiative forcing by long-lived greenhouse gases: Calculations with the AER radiative transfer models, *Journal of Geophysical Research: Atmospheres*, 113, <https://doi.org/10.1029/2008JD009944>, 2008.
- Jakub, F. and Mayer, B.: 3-D radiative transfer in large-eddy simulations – experiences coupling the TenStream solver to the UCLA-LES, *Geoscientific Model Development*, 9, 1413–1422, <https://doi.org/10.5194/gmd-9-1413-2016>, 2016.
- 680 Jänicke, B., Meier, F., Hoelscher, M., and Scherer, D.: Evaluating the effects of façade greening on human bioclimate in a complex urban environment, *Advances in Meteorology*, 14, 747259, <https://doi.org/10.1155/2015/747259>, 2015.
- Jendritzky, G., de Dear, R., and Havenith, G.: UTCI – Why another thermal index?, *International Journal of Biometeorology*, 56, 421–428, <https://doi.org/10.1007/s00484-011-0513-7>, 2012.



- Jimenez, P. A., Dudhia, J., Gonzalez–Rouco, J. F., Navarro, J., Montavez, J. P., and Garcia–Bustamante, E.: A revised scheme for the WRF  
685 surface layer formulation, *Monthly Weather Review*, 140, 898–918, <https://doi.org/10.1175/MWR-D-11-00056.1>, 2012.
- Jura, J., Novák, M., Bíla, J., Pokorný, J., and Jirka, V.: Hydrometeorological measurements to assess the effect of vegetation on urban  
microclimate, in: 2018 Smart City Symposium Prague, pp. 1–5, <https://doi.org/10.1109/SCSP.2018.8402653>, 2018.
- Kadasch, E., Sührling, M., Gronemeier, T., and Raasch, S.: Mesoscale nesting interface of the PALM model system 6.0, *Geoscientific Model  
Development*, 14, 5435–5465, <https://doi.org/10.5194/gmd-14-5435-2021>, 2021.
- 690 Kondo, J.: *Mizukankyo no kishougaku (Meteorology of water environment: Water and heat budgets at ground surface)*, Asakura Press,  
Tokyo: Japan, 1994.
- Krč, P., Resler, J., Sührling, M., Schubert, S., Salim, M. H., and Fuka, V.: Radiative Transfer Model 3.0 integrated into the PALM model  
system 6.0, *Geoscientific Model Development*, 14, 3095–3120, <https://doi.org/10.5194/gmd-14-3095-2021>, 2021.
- Krč, P., Belda, M., Bureš, M., Eben, K., Geletič, J., Radović, J., Řezníček, H., and Resler, J.: PALM-meteo 2.6: Processor of PALM meteo-  
695 rological input data, *EGUsphere*, 2025, 1–32, <https://doi.org/10.5194/egusphere-2025-4120>, 2025.
- Kubilay, A., Allegrini, J., Strelbel, D., Zhao, Y., Derome, D., and Carmeliet, J.: Advancement in Urban Climate Modelling at Local Scale:  
Urban Heat Island Mitigation and Building Cooling Demand, *Atmosphere*, 11, <https://doi.org/10.3390/atmos11121313>, 2020.
- Kusaka, H., Ikeda, R., Sato, T., Iizuka, S., and Boku, T.: Development of a Multi-Scale Meteorological Large-Eddy Simulation Model  
for Urban Thermal Environmental Studies: The “City-LES” Model Version 2.0, *Journal of Advances in Modeling Earth Systems*, 16,  
700 e2024MS004367, <https://doi.org/10.1029/2024MS004367>, 2024.
- Kántor, N., Gál, C., Gulyás, Á., and Unger, J.: The impact of façade orientation and woody vegetation on summertime heat stress pat-  
terns in a central European square: comparison of radiation measurements and simulations, *Advances in Meteorology*, p. 2650642,  
<https://doi.org/10.5194/gmd-14-5435-2021>, 2018.
- Lee, H., Mayer, H., and Schindler, D.: Importance of 3-D radiant flux densities for outdoor human thermal comfort on clear-sky summer  
705 days in Freiburg, Southwest Germany, *Meteorologische Zeitschrift*, 23, 315–330, <https://doi.org/10.1127/0941-2948/2014/0536>, 2014.
- Lehnert, M., Pánek, J., Kopp, J., Geletič, J., Květoňová, V., and Jurek, M.: Thermal comfort in urban areas on hot summer days and its  
improvement through participatory mapping: A case study of two Central European cities, *Landscape and Urban Planning*, 233, 104–113,  
<https://doi.org/10.1016/j.landurbplan.2023.104713>, 2023.
- Lindberg, F., Holmer, B., and Thorsson, S.: SOLWEIG 1.0 – Modelling spatial variations of 3D radiant fluxes and mean radiant temperature  
710 in complex urban settings, *International Journal of Biometeorology*, 52, 697–713, <https://doi.org/10.1007/s00484-008-0162-7>, 2008.
- Liu, D., Hu, S., and Liu, J.: Contrasting the performance capabilities of urban radiation field between three microclimate simulation tools,  
*Building and Environment*, 175, 106–113, <https://doi.org/10.1016/j.buildenv.2020.106789>, 2020.
- Liu, Z., Zheng, S., and Zhao, L.: Evaluation of the ENVI-Met Vegetation Model of Four Common Tree Species in a Subtropical Hot-Humid  
Area, *Atmosphere*, 9, 198, <https://doi.org/10.3390/atmos9050198>, 2018.
- 715 Maronga, B., Gryschka, M., Heinze, R., Hoffmann, F., Kanani-Sührling, F., Keck, M., Ketelsen, K., Letzel, M. O., Sührling, M., and Raasch,  
S.: The Parallelized Large-Eddy Simulation Model (PALM) version 4.0 for atmospheric and oceanic flows: model formulation, recent  
developments, and future perspectives, *Geoscientific Model Development*, 8, 2515–2551, <https://doi.org/10.5194/gmd-8-2515-2015>, 2015.
- Maronga, B., Banzhaf, S., Burmeister, C., Esch, T., Forkel, R., Fröhlich, D., Fuka, V., Gehrke, K. F., Geletič, J., Giersch, S., et al.: Overview  
of the PALM model system 6.0, *Geoscientific Model Development*, 13, 1335–1372, <https://doi.org/10.5194/gmd-13-1335-2020>, 2020.
- 720 Matuschek, O. and Matzarakis, A.: A mapping tool for climatological applications, *Meteorological Applications*, 18, 230–237,  
<https://doi.org/10.1002/met.233>, 2011.



- Matzarakis, A., Rutz, F., and Mayer, H.: Modelling radiation fluxes in simple and complex environments—Application of the RayMan model, *International Journal of Biometeorology*, 51, 323–334, <https://doi.org/10.1007/s00484-006-0061-8>, 2007.
- Matzarakis, A., Rutz, F., and Mayer, H.: Modelling radiation fluxes in simple and complex environments: basics of the RayMan model, *International Journal of Biometeorology*, 54, 131–139, <https://doi.org/10.1007/s00484-009-0261-0>, 2010.
- 725 Middel, A., Lukasczyk, J., and Maciejewski, R.: Sky View Factors from Synthetic Fisheye Photos for Thermal Comfort Routing—A Case Study in Phoenix, Arizona, *Urban Planning*, 2, 19–30, <https://doi.org/10.17645/up.v2i1.855>, 2017.
- Mlawer, E. J., Taubman, S. J., Brown, P. D., Iacono, M. J., and Clough, S. A.: Radiative transfer for inhomogeneous atmospheres: RRTM, a validated correlated-k model for the longwave, *Journal of Geophysical Research*, 102, 16 663–16 682, <https://doi.org/10.1029/97JD00237>, 1997.
- 730 Nakanishi, M. and Niino, H.: Development of an Improved Turbulence Closure Model for the Atmospheric Boundary Layer, *Journal of the Meteorological Society of Japan. Ser. II*, 87, 895–912, <https://doi.org/10.2151/jmsj.87.895>, 2009.
- Oke, T. R., Mills, G., Christen, A., and Voogt, J. A.: *Urban climates*, Cambridge University Press, <https://doi.org/10.1017/9781139016476>, 2017.
- 735 Piselli, C., Castaldo, V., Pigliautile, I., Pisello, A., and Cotana, F.: Outdoor comfort conditions in urban areas: On citizens’ perspective about microclimate mitigation of urban transit areas, *Sustainable Cities and Society*, 39, 16–36, <https://doi.org/10.1016/j.scs.2018.02.004>, 2018.
- Radović, J., Belda, M., Resler, J., Eben, K., Bureš, M., Geletič, J., Krč, P., Řezníček, H., and Fuka, V.: Challenges of constructing and selecting the “perfect” boundary conditions for the large-eddy simulation model PALM, *Geoscientific Model Development*, 17, 2901–2927, <https://doi.org/10.5194/gmd-17-2901-2024>, 2024.
- 740 Radović, J., Belda, M., Bureš, M., Eben, K., Jan, G., Jura, J., Krč, P., Řezníček, H., and Resler, J.: Dataset: Evaluating the radiative fidelity of PALM (v25.04) in high-resolution: impact of diverse urban morphology and vegetation on short-wave radiation, <https://doi.org/10.5281/zenodo.19231961>, last access: March 2026, 2026.
- Rao, V. R. and Sastri, V. M. K.: Efficient evaluation of diffuse view factors for radiation, *International Journal of Heat and Mass Transfer*, 39, 1281–1286, [https://doi.org/10.1016/0017-9310\(95\)00203-0](https://doi.org/10.1016/0017-9310(95)00203-0), 1996.
- 745 Resler, J., Krč, P., Belda, M., Juruš, P., Benešová, N., Lopata, J., Vlček, O., Damašková, D., Eben, K., Derbek, P., et al.: PALM-USM v1. 0: A new urban surface model integrated into the PALM large-eddy simulation model, *Geoscientific Model Development*, 10, 3635–3659, <https://doi.org/10.5194/gmd-10-3635-2017>, 2017.
- Resler, J., Eben, K., Geletič, J., Krč, P., Rosecký, M., Sührling, M., Belda, M., Fuka, V., Halenka, T., Huszár, P., et al.: Validation of the PALM model system 6.0 in a real urban environment: A case study in Dejvice, Prague, the Czech Republic, *Geoscientific Model Development*, 14, 4797–4842, <https://doi.org/https://doi.org/10.5194/gmd-14-4797-2021>, 2021.
- 750 Resler, J., Bauerová, P., Belda, M., Bureš, M., Eben, K., Fuka, V., Geletič, J., Jareš, R., Karel, J., Keder, J., Krč, P., Patiño, W., Radović, J., Řezníček, H., Sührling, M., Šindelářová, A., and Vlček, O.: Challenges of high-fidelity air quality modeling in urban environments - PALM sensitivity study during stable conditions, *Geoscientific Model Development*, pp. 1–35, <https://doi.org/10.5194/egusphere-2024-1231>, 2024.
- 755 Salamanca, F. and Martilli, A.: A new Building Energy Model coupled with an Urban Canopy Parameterization for urban climate simulations—part II. Validation with one dimension off-line simulations, *Theoretical and Applied Climatology*, 99, 345–356, <https://doi.org/10.1007/s00704-009-0143-8>, 2009.



- Salim, M. H., Schubert, S., Resler, J., Krč, P., Maronga, B., Kanani-Sühring, F., Sühring, M., and Schneider, C.: Importance of radiative transfer processes in urban climate models: a study based on the PALM 6.0 model system, *Geoscientific Model Development*, 15, 145–171, <https://doi.org/10.5194/gmd-15-145-2022>, 2022.
- Schoetter, R., Caliot, C., Chung, T.-Y., Hogan, R. J., and Masson, V.: Local Climate Zones for Urban Temperature Studies, *Boundary-Layer Meteorology*, 189, 103–138, <https://doi.org/10.1007/s10546-023-00827-9>, 2023.
- Skamarock, W. C., Klemp, J. B., Dudhia, J., Gill, D. O., Barker, D. M., Duda, M. G., Huang, X.-Y., Wang, W., Powers, J. G., et al.: A Description of the Advanced Research WRF Version 4, NCAR technical note, <https://doi.org/https://doi.org/10.5065/1dfh-6p97>, 2019.
- Stewart, I. D. and Oke, T. R.: Local Climate Zones for Urban Temperature Studies, *Bulletin of the American Meteorological Society*, 93, 1879–1900, <https://doi.org/10.1175/BAMS-D-11-00019.1>, 2012.
- Suter, I., Grylls, T., Sützl, B. S., Owens, S. O., Wilson, C. E., and van Reeuwijk, M.: uDALES 1.0: a large-eddy simulation model for urban environments, *Geoscientific Model Development*, 15, 5309–5335, <https://doi.org/10.5194/gmd-15-5309-2022>, 2022.
- Tewari, M., Chen, F., Wang, W., Dudhia, J., LeMone, M. A., Mitchell, K., Ek, M., Gayno, G., Wegiel, J., and Cuenca, R. H.: Implementation and verification of the unified NOAA land surface model in the WRF model, in: 20th conference on weather analysis and forecasting/16th conference on numerical weather prediction, pp. 11–15, [https://www2.mmm.ucar.edu/wrf/users/physics/phys\\_refs/LAND\\_SURFACE/noah.pdf](https://www2.mmm.ucar.edu/wrf/users/physics/phys_refs/LAND_SURFACE/noah.pdf), 2004.
- Thompson, G., Field, P. R., Rasmussen, R. M., and Hall, W. D.: Explicit Forecasts of Winter Precipitation Using an Improved Bulk Microphysics Scheme. Part II: Implementation of a New Snow Parameterization, *Monthly Weather Review*, 136, 5095 – 5115, <https://doi.org/10.1175/2008MWR2387.1>, 2008.
- Toparlar, Y., Blocken, B., Maiheu, B., and van Heijst, G. J. F.: A review on the CFD analysis of urban microclimate, *Renewable and Sustainable Energy Reviews*, 80, 1613–1640, <https://doi.org/10.1016/j.rser.2017.05.248>, 2017.
- United Nations: World Population Prospects 2024: Summary of Results, UN DESA/POP/2024/TR/NO. 9, [https://population.un.org/wpp/assets/Files/WPP2024\\_Summary-of-Results.pdf](https://population.un.org/wpp/assets/Files/WPP2024_Summary-of-Results.pdf), [cited 8.10.2025], 2024.
- Vieira Zizzo, L., Pereira Coltri, P., and Dubreuil, V.: Microscale models and urban heat island studies: a systematic review, *Environmental monitoring and assessment*, 195, 1284, <https://doi.org/10.1007/s10661-023-11906-2>, 2023.
- Wallenberg, N., Lindberg, F., Holmer, B., and Thorsson, S.: The influence of anisotropic diffuse shortwave radiation on mean radiant temperature in outdoor urban environments, *Urban Climate*, 31, 100 589, <https://doi.org/10.1016/j.uclim.2020.100589>, 2020.
- Wang, Y. and Akbari, H.: The effects of street tree planting on Urban Heat Island mitigation in Montreal, *Sustainable Cities and Society*, 27, 122–128, <https://doi.org/10.1016/j.scs.2016.04.013>, 2016.
- Watanabe, K., Kikuchi, K., Boku, T., Sato, T., and Kusaka, H.: High Resolution of City-Level Climate Simulation by GPU with Multi-physical Phenomena, in: *Network and Parallel Computing*, edited by Cérin, C., Qian, D., Gaudiot, J.-L., Tan, G., and Zuckerman, S., pp. 3–15, ISBN 978-3-030-93571-9, [https://doi.org/10.1007/978-3-030-93571-9\\_1](https://doi.org/10.1007/978-3-030-93571-9_1), 2022.
- World Meteorological Organization: Guide to Instruments and Methods of Observation, Volume III – Observing Systems, WMO-No. 8, <https://doi.org/10.59327/WMO/CIMO/3>, [cited 8.10.2025], 2024.
- Yang, S., Wang, L., Stathopoulos, T., and Marey, A. M.: Urban microclimate and its impact on built environment – A review, *Building and Environment*, 238, 110 334, <https://doi.org/10.1016/j.buildenv.2023.110334>, 2023.